A new view on gold speciation in sulfur-bearing hydrothermal fluids from in situ X-ray absorption spectroscopy and quantum-chemical modeling

Gleb S. Pokrovski, Boris R Tagirov, Jacques Schott, Jean-Louis F Hazemann, Olivier Proux

A new view on gold speciation in sulfur-bearing hydrothermal fluids from in situ X-ray absorption spectroscopy and quantum-chemical modeling

Gleb S. Pokrovski [1,2,3] *, Boris R. Tagirov [4,7], Jacques Schott [1,2,3],

Jean-Louis Hazemann [5], and Olivier Proux [6]

1- Université de Toulouse, UPS, OMP, 14 avenue Edouard Belin, F-31400 Toulouse, France

2- CNRS, LMTG, Laboratoire des Mécanismes et Transferts en Géologie, F-31400 Toulouse, France

3- IRD, LMTG, F-31400 Toulouse, France

4 - Institut für Mineralogie und Petrographie, ETH Zurich, CH 8092 Zurich, Switzerland

5- Institut Néel, CNRS, 25 avenue des Martyrs, F-38042 Grenoble Cedex 9, France

6- Observatoire des Sciences de la Terre, de l'Univers et de l'Environnement de Grenoble, 414 rue de la piscine, F-38400 St Martin d'Hères, France

7- Institute of Ore Deposit Geology, IGEM RAS, 35 Staromonetniy per., 119017 Moscow, Russia

* *Corresponding author*:
Phone: (33)-(0)5-61-33-26-18; fax: (33)-(0)5-61-33-25-60; E-mail: pokrovsk@lmtg.obs-mip.fr

Running title: Gold in sulfur-bearing hydrothermal fluids

Keywords: gold; sulfur; hydrothermal fluid; XAFS spectroscopy; Au-S complexes; quantum-chemical modeling, thermodynamic properties

Geochimica et Cosmochimica Acta - W6365

Revised version, June 2009

ABSTRACT

Despite the common belief that Au^I complexes with hydrogen sulfide ligands (H_2S/HS^-) are the major carriers of gold in natural hydrothermal fluids, their identity, structure and stability are still subjects of debate. Here we present the first in situ measurement, using X-ray absorption fine structure (XAFS) spectroscopy, of the stability and structure of aqueous Au^I-S complexes at temperatures and pressures (*T-P*) typical of natural sulfur-rich ore-forming fluids. The solubility of native gold and the local atomic structure around the dissolved metal in S-NaOH-Na_2SO_4-H_2SO_4 aqueous solutions were characterized at temperatures 200-450°C and pressures 300-600 bar using an X-ray cell that allows simultaneous measurement of the absolute concentration of the absorbing atom (Au) and its local atomic environment in the fluid phase. Structural and solubility data obtained from XAFS spectra, combined with quantum-chemical calculations of species geometries, show that gold bis(hydrogensulfide) $Au(HS)_2^-$ is the dominant Au species in neutral-to-basic solutions ($5.5 \leq pH \leq 8.5$; H_2O-S-NaOH) over a wide range of sulfur concentrations ($0.2 < \Sigma S < 3.6$ mol/kg), in agreement with previous solubility studies. Our results provide the first direct determination of this species structure, in which two sulfur atoms are in a linear geometry around Au^I at an average distance of 2.29±0.01 Å. At acidic conditions ($1.5 \leq pH \leq 5.0$; H_2O-S-Na_2SO_4-H_2SO_4), the Au atomic environment determined by XAFS is similar to that in neutral solutions. These findings, together with measured high Au solubilities, are inconsistent with the predominance of the gold hydrogensulfide $Au(HS)^0$ complex suggested by recent solubility studies. Our spectroscopic data and quantum-chemical calculations imply the formation of species composed of linear S-Au-S moieties, like the neutral [H_2S-Au-SH] complex. This species may account for the elevated Au solubilities in acidic fluids and vapors with H_2S concentrations higher than 0.1-0.2 mol/kg. However, because of the complex sulfur speciation in acidic solutions that involves sulfite, thiosulfate and polysulfide species, the formation of Au^I complexes with these ligands (e.g., $AuHS(SO_2)^0$, $Au(HS_2O_3)_2^-$, $Au(HS_n)_2^-$) cannot be ruled out. The existence of such species may significantly enhance Au transport by high *T-P* acidic ore-forming fluids and vapors, responsible for the formation of a major part of the gold resources on Earth.

1. INTRODUCTION

Knowledge of the identity, structure and stability of aqueous gold complexes is required for the quantitative assessment of Au transport, distribution, and deposition by hydrothermal fluids in the Earth's crust, and for effective, low-cost, and safe extraction of gold from its ores. Currently available data show that hydrogen sulfide and sulfide (H_2S, HS^-, S^{2-}) complexes of aurous gold (Au^I) are the major carriers of this metal both in ore-bearing fluids that formed most gold porphyry and epithermal deposits, and in geothermal waters from active volcanic areas (e.g., Seward, 1989; Stefánsson and Seward, 2004; references therein). Until now, however, there has been no spectroscopic characterization of Au^I-sulfide aqueous complexes in aqueous solution at elevated temperatures, and all available information on their stoichiometry and stability stems from solubility measurements.

Most existing solubility data, since the pioneering work of Seward (1973), indicate that gold bis(hydrogensulfide) $Au(HS)_2^-$ is likely to be the dominant Au species in near-neutral (4-5 $\leq pH \leq$ 8-9) solutions over wide temperature and pressure (*T*-*P*) ranges (e.g., see Fig. 1 and Stefánsson and Seward, 2004; Tagirov et al., 2005, 2006; Akinfiev and Zotov, 2001; Akinfiev et al., 2008 for reviews of available Au speciation data). In contrast, the stoichiometry and stability of Au-S complexes formed at acidic *pH* still remain a matter of controversy. For example, if many recent solubility studies carried out at *T* 100-500°C and *P* to 1 kbar suggest the formation of the hydrogensulfide $AuHS^0$ complex at $pH \leq$ ~5 and H_2S concentrations $\leq$ ~ 0.2 mol/kg, the reported stability constants for this species display variations up to 2 orders of magnitude in the studied *T*-*P* range (e.g., Benning and Seward, 1996; Gibert et al., 1998; Stefánsson and Seward, 2004; Tagirov et al., 2005). Few solubility studies carried out at higher H_2S concentrations (to ~0.5 mol/kg of fluid, e.g., Hayashi and Ohmoto, 1991) or higher temperatures and pressures (500-700°C, 1-4 kbar, Loucks and Mavrogenes, 1999) suggest the

dominant formation of other species at acidic conditions, like $HAu(HS)_2^0$ or $AuHS(H_2S)_3^0$, respectively.

Surprisingly, little attention has been devoted to Au complexing with aqueous sulfur ligands other than hydrogen sulfide, like thiosulfate and polysulfides that form in hot springs and fumaroles or during bacterial activity in moderate-temperature (< 100°C) past and present hydrothermal and volcanic settings (e.g., Berndt et al., 1994; Migdisov and Bychkov, 1998; Lengke and Southam, 2006). Furthermore, the impact on gold transport of sulfite (SO_2), which often dominates over sulfide (H_2S) in magmatic fluids at oxidizing conditions typical of active convergent margins (e.g., Hedenquist and Lowenstern, 1994; Borisova et al., 2005, 2006) and in volcanic gases (e.g., Wallace, 2001), has been ignored until very recently (e.g., Pokrovski et al., 2008a).

Because of the complex chemistry of sulfur in natural fluid systems and the experimental difficulties inherent to the implementation of solubility or synthetic fluid-inclusion methods, in situ spectroscopic data on Au-S interactions in high *T-P* fluids may provide new insights into the identity, stoichiometry and stability of the species controlling the Au transport. Such spectroscopic approaches have recently become possible owing to the progress in synchrotron radiation techniques and optical cell design (e.g., Seward and Driesner, 2004; Testemale et al., 2005), and new developments in quantum chemical and molecular dynamics simulations of species structures (e.g., see Sherman, 2001, for review). In addition, quite recently a number of in situ spectroscopic studies involving *simultaneous measurement* of solid phase solubilities and local atomic structures of solutes in hydrothermal fluids has been reported using Raman and X-ray absorption spectroscopy techniques (e.g., Zotov and Keppler, 2002; Pokrovski et al., 2005a, 2006, 2008b, 2009).

Here we present in situ X-ray absorption fine structure (XAFS) spectroscopy measurements of gold solubility, speciation, and structure in S-bearing aqueous fluids to 450°C

and 600 bar in model systems $Au_{(s)}$-H_2O-S-H_2SO_4-Na_2SO_4-NaOH allowing to cover a wide range of *pH* (1.5-8.1) and S aqueous speciation. Spectroscopic results were combined with quantum chemical calculations of optimized geometries of aqueous species and thermodynamic analyses of available solubility data to investigate the stability and structure of the major Au-S aqueous complexes at elevated temperatures. The results provide new insights into the geochemistry of gold and, in particular, the role of different sulfur ligands in Au transport by S-rich ore-bearing fluids in hydrothermal-magmatic settings.

2. MATERIALS AND METHODS

2.1. XAFS spectra acquisition and reduction

XAFS spectra (including the X-ray absorption near-edge structure region or XANES, and the extended X-ray absorption fine structure region or EXAFS) on Au aqueous solutions were collected in both transmission and fluorescence mode at Au L_3-edge (11.919 keV) at BM30b-FAME beamline (Proux et al., 2005) of the European Synchrotron Radiation Facility (ESRF, Grenoble, France). The storage ring was operated at 6 GeV with a ~200 mA current. Energy was selected using a Si(220) double-crystal monochromator with dynamic sagittal focusing, yielding a beam spot on the sample of ~300 μm horizontal × 200 μm vertical and an X-ray photon flux of ~10^{12} photons/s, allowing acquisition of good quality EXAFS spectra at Au concentrations as low as 10^{-3} mol/kg. Silicon diodes collecting scattered radiation from a Kapton foil were employed for measuring the intensities of incident and transmitted X-rays. Fluorescence spectra were collected in the right-angle geometry using a Canberra 30-element solid-state germanium detector. Energy was constantly calibrated using a gold metal foil; its L_3 edge energy was set at 11.919 keV as the maximum of the first derivative of the main edge spectrum. More details about the beamline and X-ray setup may be found elsewhere (Pokrovski et al., 2006, 2009; Proux et al., 2006; Tella and Pokrovski, 2009).

Experiments were carried out using a high *T-P* cell developed at the Institut Néel (Testemale et al., 2005) and described in detail elsewhere (see Electronic annex EA1 and Pokrovski et al., 2005a, 2006, 2008b, 2009). The apparatus includes an inner glassy-carbon cell heated by electrical resistances and inserted in a stainless steel vessel pressurized with helium and equipped with a water-cooling jacket and three beryllium windows for X-ray passage. The internal cell consists of a vertical glassy carbon tube and two coaxial sapphire rods equipped with Viton O-ring seals and inserted into the tube from each end. The rods delimit the sample space, in which the experimental solution and solid are placed, and can move in the tube in response to *T-P* changes as a piston in a syringe. This design enables accurate absorption measurements in transmission mode allowing determination of both dissolved metal and sulfur concentrations, and in fluorescence mode to obtain higher quality EXAFS spectra at Au L_3 edge to extract structural information.

EXAFS data analysis was performed with the HORAE and IFEFFIT programs (Ravel et al., 2005) and following the recommendations of the International XAFS Society (Sayers, 2000). Dissolved Au concentrations were determined from the amplitude of the absorption edge height of the Au L_3-edge transmission spectra using the classical X-ray absorption relation. Total sulfur concentration was roughly estimated from the before-edge absorbance of the fluid phase as measured in transmission mode. Details about the reduction procedure and concentration measurements can be found in EA-1 and Pokrovski et al. (2008b, 2009).

2.2. Experimental methodology and conditions

Gold dissolution experiments were performed in the systems S-NaOH-H_2O (4 runs), S-H_2O (4 runs) S-Na_2SO_4-H_2O (2 runs), and S-H_2SO_4-H_2O (1 run) by allowing a piece of gold foil (99.99% purity, 30-60 mg, diameter 2-3 mm, thickness 0.5mm) and a sulfur crystal (99.999% purity, 1-5 mg) to react with the given aqueous solution at high *T-P*. Initial gold-to-solution mass ratio was about 1:4. Gold and sulfur dissolution was monitored by measuring in transmission mode the spectral absorption-edge jump and before-edge absorbance as a function of time at constant pressure of 300 or 600 bar and *T* steps of 50-100°C from 200 to 450°C (see EA-1). Simultaneously, fluorescence spectra were recorded from the fluid phase. Five to twenty scans of ~40 min/scan (depending on dissolved Au concentration) were

collected and then averaged together at each *T*-*P* point after attainment of a steady-state Au concentration.

The use of elemental sulfur as starting material allows in situ generation of high concentrations of sulfide ligands at elevated temperature, and efficient redox and *pH* buffering of the system through the sulfate-sulfide equilibrium, providing oxygen fugacities close to those of the magnetite-hematite mineral buffer. Such oxidizing conditions are favorable for gold dissolution, yielding relatively high dissolved Au concentrations measurable by XAFS spectroscopy (Fig. 1). Thermodynamic equilibrium calculations (see Appendix) and available sulfur solubility experiments (e.g., Ellis and Giggenbach, 1971; Robinson, 1973; Ohmoto and Lasaga, 1982) indicate that at near-neutral conditions ($6<pH<9$), the reaction of elemental sulfur with NaOH-H_2O solutions above 200°C produces mainly sulfide (H_2S, $NaHS^0$, HS^-) and sulfate ($NaSO_4^-$, HSO_4^-, SO_4^{2-}) species. At slightly acidic *pH* (S-Na_2SO_4, *pH* ~ 4-5), thermodynamic calculations at $T \geq 300$°C suggest H_2S and sulfate species ($NaSO_4^-$, HSO_4^-, SO_4^{2-}) to be dominant, with only minor amounts of SO_2 (~ 1%, Fig. 2).

In contrast, in more acidic solutions ($pH \leq 4$), the sulfur speciation is less constrained. The major reason for that is the very fast equilibration kinetics between different sulfur redox forms at acidic *pH* (Ohmoto and Lasaga, 1982) leading to rapid recombination of these species upon changing *T* or solution composition, thus making delicate the use of classical sampling or quenching techniques and hampering accurate analyses at ambient conditions. Although calculations using the SUPCRT database (Johnson et al., 1992) predict H_2S and SO_2 to be the largely dominant sulfur forms at $pH \leq 3$ at our experimental conditions (Fig. 2), solubility (Sorokin and Dadze, 1994) and in situ Raman spectroscopy (Bondarenko and Gorbaty, 1997) measurements in the S-H_2O system at 300-500°C show the formation, in addition to H_2S and SO_2, of significant amounts of zero-valent sulfur (S_n), polysulfides ($H_{0-2}S_n$) and thiosulfates ($H_{0-2}S_2O_3$), but their degree of protonation and concentrations are poorly constrained, and no robust thermodynamic data are available for these species at $T \geq 100$°C. This yields uncertainties of $\geq 50\%$ for sulfur solubilities in acidic solutions above 250°C. The distribution of the dominant S species derived from different data sources for typical conditions of our experiments is summarized in Fig. 2, and more details are presented in Table A1.

Total dissolved sulfur concentrations ranged from ~ 0.2 to 4 m[1] in our experiments as roughly estimated from the before-edge absorbance (see EA-1 and Pokrovski et al., 2008b for details); they are in reasonable agreement, within ~50%, with the predicted sulfur solubilities. In most experiments, both sulfur and gold aqueous concentrations reach a steady-state within a few hours. In some high-temperature runs ($\geq$ 400°C) performed in S-rich solutions, their concentrations start to decrease slightly after several hours, likely owing to precipitation of some amounts of sulfur in colder parts of the cell close to the Viton seals and fluorescence window. Nevertheless, this had no detectable effect on the structural parameters derived from XAFS spectra.

2.3. Quantum-chemical calculations

Quantum chemical calculations of optimized structures of Au-S species were performed using the Gaussian 03 - Revision C.02 suite of programs (Frisch et al., 2004). The 2nd-order Møller-Plesset Perturbation Theory (MP2) and Density Functional Theory (DFT, Becke, 1993) with the B3LYP functional were employed. In a previous paper (Pokrovski et al., 2009), we found the MP2 method to give a better agreement with the experimental Au-Cl distances than the DFT approach. Therefore, in the present study most calculations were performed with the MP2 method, and a few selected species were also tested with DFT. Default Gaussian's convergence criteria were adopted for geometry optimizations and energy calculations. The 6-311++G(d,p) basis set was applied to H, O, and S. A relativistic effective core potential (RECP) suggested by Schwerdtfeger et al. (1989) was used for Au. This potential, combined with the [7s,3p,4d] contraction of valence electrons, was used to approximate the Au inner electronic structure consisting of 60 electrons ([Kr] + 4d + 4f). Feller et al. (1999) in their study of hydration of Cu^+, Ag^+, and Au^+ noted that a single set of *f* functions added to the Cu valence basis set yielded significantly shorter Cu-O distances (by ~0.03 Å) than calculations without this function. Therefore, a series of calculations for $Au(HS)_2^-$ was performed using the [7s,3p,4d,1f] contraction for Au valence electrons with the Gaussian exponent $\zeta_f = 1$ as optimized by Feller et al. (1999). In contrast to the Cu-O distances, adding this *f*-type polarization function resulted in insignificant decrease of the Au-S distance ($\leq$ 0.009 Å). Calculations in aqueous solution were carried out using the Conductor-like

[1] m denotes molality (i.e. the number of moles of solute per kg of water in solution) through the entire article.

Polarized Continuum Model (CPCM, see Takano and Houk, 2005 for the review and benchmarking of this method), with a dielectric constant ε of 78.3 corresponding to that of pure water at 25°C and 1 bar. The values of dielectric constant used in the CPCM calculations and in those for the gas phase (ε = 1) cover the wide range of solvent properties corresponding to the *T-P* conditions of our XAFS experiments (ε = 10-30). All optimized geometries were characterized as stationary points on the potential energy surface via vibrational frequency calculations (no imaginary frequencies). Optimizations of the $HAu(HS)_2^0$ geometry with H bounded directly to the Au atom yielded a first-order saddle point with an H-Au-S angle of ~90°. However, when starting with an initial angle value only very slightly different from 90° (by ~1°), calculations always converged to the linear [H_2S-Au-SH] geometry shown in Fig. 3.

3. RESULTS

3.1. Results of quantum-chemical calculations

Calculated Au-S and Au-O interatomic distances and bond angles of the selected Au complexes are presented in Table 1, and the optimized species geometries are shown in Fig. 3. The following observations can be drawn from these results.

a) The average value of the Au-S distance is 2.33±0.06 Å as calculated from all Au-S species considered (here the uncertainty represents the maximum variation from the average value of distances in the different species examined).

b) There are two stationary points corresponding to the stoichiometries $AuHS(H_2S)$ and $AuHS(H_2O)$, with different positions of protons relatively to the S-Au-S or S-Au-O axis (Fig. 3). We denote these structures as *cis* and *trans* isomers. Their stabilities are very similar, with differences in their SCF energies not exceeding 0.1 kcal/mol.

c) Changes in dielectric constant (ε) have a detectable effect on the complex geometries. For example, the change of ε from the gas phase (ε=1) to the aqueous solution at 25°C and 1

bar (ε=78.3) for the $AuHS(H_2O)^0$ complex causes an increase of the Au-S distance by ~ 0.015 Å, and a contraction of the Au-O distance by 0.05 Å. The evolution of the Au-SH and Au-SH_2 distances in $AuHS(H_2S)^0$ with ε is similar, exhibiting a slight increase in $R_{Au\text{-}SH}$ and a decrease in $R_{Au\text{-}SH_2}$ from the gas phase to the aqueous solution. In contrast, $Au(HS)_2^-$ shows a contraction by 0.01 Å of its both Au-S distances when passing from gas to solution. Bryce et al. (2003) calculated an Au-S distance of 2.355 Å for $Au(HS)_2^-$ at 25°C using the COSMO/SD+(Au)/6-31+G(d)(S,H) level of theory. This compares favorably with the values of 2.327 and 2.365 Å obtained in the present study at ε = 78.3 using the MP2 and DFT methods, respectively.

3.2 Results from XANES spectra

XANES spectra (Fig. 4) of all S-bearing solutions *at near-neutral pH (S-NaOH-H_2O)* exhibit close shapes, amplitudes, and energies of absorption edge at 11920.0±0.5 eV (defined as the maximum of the edge first derivative of the spectrum) over the whole *T-P* and sulfur concentration range. The spectral general features are similar to crystalline Au^I sulfide and thiosulfate solids in which gold is linearly coordinated with two S ligands in the nearest shell. Two-coordinate linear geometries for Au^I are also typical for its solid compounds and aqueous complexes with other ligands like P and Cl (e.g., Benfield et al., 1994; Pokrovski et al., 2009). The spectra of Au-S solutions show no detectable features of metallic gold or trivalent Au^{III}, thus demonstrating the dominant presence of monovalent Au^I in the studied systems.

XANES spectra recorded from *acidic S-H_2O and S-Na_2SO_4-H_2O solutions* between 200 and 450°C are similar in the *pH* range 2-5 but present subtle differences with spectra at neutral *pH*. This indicates a similar Au nearest atomic environment between neutral and acidic *pH*, in a linear coordination with 2 sulfur ligands, but likely a different next-nearest coordination. The examination of Fig. 4 reveals a slight growth in amplitude of the resonance at ~11923 eV with decreasing *pH* (feature A). This feature is particularly pronounced in the Au^I thiosulfate

aqueous complex, $Au(S_2O_3)_2^{3-}$, investigated in this work (Table 3) and previous studies (Bryce et al., 2003). Another resonance at ~11929 eV (feature B in Fig. 4) exhibits an opposite evolution, with its amplitude slightly decreasing from neutral (exp #2, 3) to acidic (exp #5, 8) *pH* and further weakening in the spectra of the Au^I thiosulfate solid and aqueous complex. This is accompanied by a systematic shift, by 1-2 eV, of its maximum towards higher energies. These spectral trends might indicate the presence in acidic high *T-P* solutions of complexes containing other S/O atoms in the Au next-nearest coordination shell like in Au-thiosulfate, in addition to the first-shell S-Au-S entity detectable by EXAFS (see below). It should be noted, however, that XANES spectra may also be affected by charge transfers between the metal and ligand, whose amplitude and direction depend on the electrical charge of the complex and the number and position of protons (e.g., Testemale et al., 2004). Consequently, a change in the charge of the dominant Au-S complexes from neutral to acid *pH* (e.g., $Au(HS)_2^-$ to $Au(H_2S)(HS)^0$) might also affect the position and amplitude of XANES features. A quantitative analysis of XANES spectra using ab-initio quantum chemical modeling will be provided in a future contribution.

3.3 Results from EXAFS spectra

EXAFS spectra *of slightly acidic to neutral solutions* (Fig. 5) are consistent with the presence of ~2 sulfur atoms at an average distance of ~2.29 Å from Au in the nearest shell (Table 2). These parameters remain constant within errors in the whole range of investigated temperature and sulfur concentration. The Au-S distances in high *T-P* S-bearing solutions determined in this study are similar within ~0.02 Å to those found in Au^I sodium thiosulfate salt and the $Au(S_2O_3)_2^{3-}$ aqueous complex (Bryce et al., 2003; this study, Table 3), as well as in many Au^I organic thiolates (e.g., Elder and Eidsness, 1987; Bishop et al., 1998) that contain linear AuS_2 units characteristic of the Au^I coordination chemistry (Cotton and Wilkinson,

1988). The linear geometry S-Au-S in S-rich high-*T* solutions is also consistent with the small feature apparent in the Fourier Transform of EXAFS spectra at ~4 Å (not corrected for phase shift, Fig. 5). This contribution was successfully modeled using order-3 and -4 multiple scattering paths within the linear S-Au-S' cluster like Au-S-S'-Au and Au-S-Au-S'-Au ($R_{ms} = 2\times R_{Au-S}$) as predicted by FEFF calculations. The fitted Debye-Waller factors for these paths were found to be about two times greater than those for the corresponding Au-S single-scattering path, thus further supporting a linear S-Au-S geometry in the aqueous complexes.

EXAFS spectra of *acidic solutions* are very similar to those in near-neutral solutions (Fig. 5), and are largely dominated by the first-shell contribution from two sulfur atoms at 2.29±0.01 Å (Table 2). It should be emphasized that, according to all available thermodynamic data, $Au(HS)_2^-$ is present in negligible amounts ($\leq$ a few % of total dissolved Au) at $pH \leq 3$ and sulfur concentrations of this study (Fig. 1, section 4.2), and $AuHS^0$ is widely believed to be the dominant Au species in sulfide acid solutions, on the basis of extensive batch-reactor solubility measurements (e.g., Stefánsson and Seward, 2004; Tagirov et al., 2005; references therein). The presence of two S atoms in the Au first coordination shell is inconsistent with the neutral mono-sulfide complex. Our quantum chemical geometry optimizations for this complex predict a two-fold linear coordination of Au with an HS^- ligand and a water molecule with Au-S and Au-O distances of 2.26-2.28 and 2.15-2.20 Å, respectively (Table 1, Fig. 3). The experimental EXAFS spectra are, however, irreconcilable with the presence of O atoms at distances from 1.8 to 2.5 Å. Inclusion of oxygen in the model yielded poor and unstable fits either with Au-O amplitudes tending to zero (within ±0.2 O atoms) or unphysical large Au-O DW factors ($\sigma^2 \sim$ 0.05-0.1 $Å^2$) if the number of oxygen atoms is constrained to ~1 assuming the predominance of $Au(H_2O)(HS)^0$. Thus, the two-fold Au-S coordination clearly implies the dominant presence, in acidic S-rich solutions, of species other than the hydrogen sulfide complex $AuHS^0$.

3.4 Results from solubility measurements

Steady-state Au concentrations in solution as measured by monitoring the Au absorption edge-height in transmission mode as a function of time are attained within less than 1-2 hours at temperatures 200 to 450°C and pressures 300 and 600 bar in all experiments *in the Au-H_2O-NaOH-S system* (exp #1 to 4, e.g. Fig. 6a,b). Dissolved sulfur concentrations estimated using the before-edge absorption also show only weak evolution with time at a given *T-P*, suggesting likely attainment of equilibrium. The only exception is exp #2 at 450°C where dissolved S concentrations decreased by ~50% in less than 2 hours (Fig. 6), probably due to sulfur condensation in colder parts of the cell. Dissolved Au concentrations measured in this study are reported in Table 4, and compared in Table A2 with Au solubilities calculated for each experimental *T-P* point using available literature data (see Appendix for discussion of data sources, original experimental conditions and uncertainties).

Dissolved Au concentrations *in acidic H_2O-S(-H_2SO_4) solutions (exp #5-8 and 11, $1.5<pH_{calc}<3.0$)* show large variations and poor reproducibility in different runs, ranging from ~ 10^{-4} (detection limit) to 5×10^{-3} m (Fig. 7a). In most runs conducted in the S-H_2O system and in a single run in the presence of H_2SO_4, Au concentrations are close to or below 2×10^{-4} m, and show no detectable dependence on *T* (from 300 to 450°C) or time (from 2 to 16 h at a given *T*). The only exception is exp #5 (H_2O-1.0 m S) that yielded mean dissolved Au concentrations of 10^{-3} and 5×10^{-4} m at 300 and 400°C, respectively (Fig. 7a, Table 4). At 300°C in this experiment, the scatter between $\Delta\mu$ values from different XAFS scans attains, however, a factor of 4. This may suggest that equilibrium was likely not attained at that temperature.

Dissolved gold concentrations, measured *in H_2O-S-Na_2SO_4 solutions (exp # 9 and 10) at pH between 4 and 5*, attain a steady state within less than 2 hours at 400°C in both experiments, remain almost constant for at least 5 hours, and then display a detectable decrease (Fig. 7b). At 300°C, Au concentrations exhibit a large increase during the first two hours, and then decrease

to an almost constant value. Such kinetic pattern might be related to the slow sulfur dissolution and equilibration between its different species. Our spectroscopically measured solubilities are compared with available literature data in section 4.2 below.

4. DISCUSSION

4.1 Gold speciation as inferred from XAFS spectroscopy

4.1.1. H_2O-S-NaOH and H_2O-S-Na_2SO_4 solutions at slightly acidic to neutral pH (5-8)

The structural parameters for aqueous gold and Au solubilities measured in this study are consistent with the dominant formation of the linear Au^I-hydrosulfide species, $Au(HS)_2^-$, in neutral sulfide-bearing aqueous solutions over the investigated temperature (200-450°C) and sulfide concentration ranges (0.05-2.0 m H_2S/HS^-) of this study, as inferred from available solubility data (section 4.2). The Au-S distances in $Au(HS)_2^-$, predicted by quantum-chemical calculations in this work (section 3.1) and previous studies (Tossel et al., 1996; Bryce et al., 2003), are systematically larger, by 0.04-0.10 Å, than those derived from our EXAFS spectra. This disagreement might, at least partly, be explained by the deficiency of the Au basis set used in quantum-chemical calculations and, probably, by insufficient account of hydration effects in solution using the CPCM model.

Note that because of the weak EXAFS signal from hydrogen atoms, their presence cannot be detected in most cases. No other next-nearest single-scattering contributions which might arise from outer-sphere oxygen atoms of water molecules or S/Na/Au atoms beyond the first shell were detected within the limits of spectral resolution, thus indicating the absence of significant hydration, polymerization or ion-pairing in the Au-S-NaOH aqueous solutions. However, because of the strong damping of EXAFS signal by both structural and thermal disorder, the presence of loosely bound and disordered second-shell neighbors cannot be

completely excluded on the solely basis of XAFS spectroscopy. Although our ab-initio calculations predict the presence of H_2O and H_2S molecules at distances greater than 3-4 Å from the gold atom in the outer coordination shells of the $Au(HS)_2^-$ species, such weak outer-sphere solvation has almost no influence on the first-shell structure of this species. Thus, the constancy of the Au-S average bond length and low DW factors over the wide temperature range imply that, due to the strong covalent character of the Au-S bonds, the increasing thermal disorder and changes in the solvent properties with temperature have no significant effect on the structure of Au sulfide species.

4.1.2. H_2O-S solutions at acidic pH (2-4)

The shape and energy position of XANES spectra and the structural parameters from EXAFS spectra for aqueous gold in acidic S-rich solutions clearly imply the dominant presence of complexes composed of S-Au-S units, which is inconsistent with the $AuHS^0$ complex suggested in available solubility works. Below we discuss the stoichiometry of possible gold species, which may or may not be compatible with the structural results obtained in this study in acidic solutions.

Loucks and Mavrogenes (1999) suggested the formation of a tetrakis(hydrogensulfide) complex $AuHS(H_2S)_3^0$ at acidic *pH* from their gold solubility experiments in the presence of the pyrite+pyrrhotite±magnetite assemblage at *T* 550-725°C and *P* 1-4 kbar. If such a species involves 4 S ligands in the nearest coordination shell of Au, its formation in the present study would be inconsistent with *a)* the average number of two for S neighbors measured in acidic solutions, *b)* the energy position, shape, and amplitude of XANES spectra which imply a two-fold Au-ligand coordination, and *c)* the absence of known aurous tetra-coordinated compounds with sulfur. Alternatively, the tetra-sulfide complex of Loucks and Mavrogenes (1999) might be constituted of an HS^- and H_2S ligand in the Au inner-sphere shell and of two other H_2S

ligands in the outer-sphere shell, yielding a stoichiometry $(HS)Au(SH_2)\cdot 2H_2S$. In that case, neither XANES nor EXAFS would enable detection of the outer-sphere sulfur atoms. However, the formation of such a complex in our experiments is supported neither by quantum chemical calculations, which indicate only very weak solvation of Au bisulfide species by outer-sphere H_2S molecules, nor by measured solubilities (see section 4.2).

A more likely candidate would be the neutral $Au(H_2S)(HS)^0$ species proposed in solubility studies of Hayachi and Ohmoto (1991) performed in S-Na_2SO_4 aqueous solutions similar to those used in our study, and of Wood et al. (1987) in the presence of a Fe-Zn-Pb-Sb-Ag-Mo-Bi sulfide mineral assemblage. Such a stoichiometry is compatible with *a)* the elevated S concentrations ($\geq$ 0.2m) in our low-*pH* XAFS experiments in comparison to those corresponding to the $AuHS^0$ predominance domain (at $\leq$ ~0.1m H_2S) according to previous solubility measurements, and *b)* the two-fold Au-S coordination found from XAFS spectra. Our quantum-chemical calculations of this complex structure predict a linear S-Au-S configuration with Au-(SH_2) and Au-(SH) distances of ~2.37 and ~2.28 Å, respectively (Table 1). Such a distance splitting could not, however, be resolved by EXAFS within spectral statistics because of the limited exploitable k-range of the spectra (Δk ~8-10 $Å^{-1}$) that fixes the distance resolution ΔR for two equivalent sub-shells at ~0.15-0.2 Å according to the formula $\Delta R = \pi/2\Delta k$ (Teo, 1986). Note that the average value of R_{Au-S} predicted by quantum chemical calculations in the neutral bis(hydrogensulfide) species is only 0.04 Å larger than the experimental EXAFS distance; this difference is similar to that found for the $Au(HS)_2^-$ complex.

Because of the growing fraction of SO_2 with both increasing *T* and decreasing *pH* in S-H_2O solutions as shown by thermodynamic calculations (Fig. 2, Table A1), Au bis(sulfite) and/or "mixed" sulfite-sulfide species might also account for the obtained XAFS structural parameters. Calculations of optimized geometries for $Au(HSO_3)_2^-$ and $Au(HS)(SO_2)^0$ yield a mean Au-S distance in the sulfite species (~2.33 Å) identical to that in $Au(H_2S)(HS)^0$, and in

the sulfide-sulfite species (~2.28 Å) very close to the XAFS distance, with a small difference between Au-SH and Au-SO_2 bond lengths ($\leq$ 0.01 Å, Table 1). Neither such a distance splitting nor the presence of oxygen atoms belonging to the SO_2 ligand in the next-nearest atomic shell of Au (expected at 3.2-3.6 Å from the central Au atom) are resolvable in our EXAFS spectra.

The Au-S structural parameters derived from XAFS spectra in acidic solutions may also be consistent with the formation of Au thiosulfate or polysulfide species. Although the lack of thermodynamic data does not allow reliable prediction of their amounts at elevated *T-P*, the presence of such sulfur forms was revealed both by solubility and spectroscopic measurements in the S-H_2O system at conditions similar to our experiments. For example, thiosulfate concentrations between 0.001 and 0.01 m were reported by Sorokin and Dadze (1994) from chemical analyses of the sampled aqueous fluid in equilibrium with liquid sulfur in batch-reactor experiments at 200-450°C and 300-500 bars (Fig. 2). Given the great stability of the $Au(S_2O_3)_2^{3-}$ complex at ambient conditions ($\log_{10}\beta\,(Au(S_2O_3)_2^{3-})$ = 28.0 [2], Skibsted and Bjerrum, 1977), such thiosulfate concentrations are potentially sufficient to complex all dissolved gold in our experiments in acidic solutions. In situ Raman spectroscopy measurements of Bondarenko and Gorbaty (1997), carried out between 200 and 500°C at 1000 bar on pure water saturated with sulfur, revealed the growth with *T* of bands tentatively attributed to $H_nS_2O_3^{n-2}$, S_8 or H_2S_n species. Thermodynamic calculations based exclusively on low-*T* data are likely to largely underestimate the thiosulfate and polysulfide formation at our experimental conditions, predicting concentrations less than 10^{-3}-10^{-4} m (Table A1). Gold complexes with such ligands would involve a [-S-S-Au-S-S-] moiety, and thus contain sulfur atoms in the Au second coordination shell. A second S shell could not be detected unambiguously in our EXAFS spectra. It should be emphasized, however, that its detection is difficult due to both the large disorder associated with such bonds and the overlap of their

[2] β denotes the thermodynamic equilibrium constant for the reaction: $Au^+ + 2S_2O_3^{2-} = Au(S_2O_3)_2^{3-}$

EXAFS signal with that from the strong linear multiple-scattering paths within the [S-Au-S] unit. Note that a second sulfur shell could not be detected unambiguously within spectral statistics at ambient conditions in the aqueous $Au(S_2O_3)_2^{3-}$ complex; this shell exhibits a very weak amplitude and large disorder even in the spectrum of crystalline Au thiosulfate (Table 3). The presence of S, and eventually O, in the next-nearest Au shell in H_2O-S(-Na_2SO_4) solutions seems to be supported by XANES spectra (see above), which are more sensitive to the cluster geometry and symmetry and less affected by the disorder than EXAFS.

4.2 Gold speciation as inferred from solubility measurements

4.2.1. H_2O-S-NaOH solutions at near-neutral to slightly basic pH (6-8)

Gold concentrations at near-neutral *pH* derived from XAFS spectra are in good agreement, within 0.1-0.5 log unit in the 200-450°C range, with the solubility data of Shenberger and Barnes (1989), Fleet and Knipe (2000) and Dadze et al. (2000). The experimental conditions and sulfur sources vary greatly in these studies (e.g., H_2S-Na_2SO_4, S-NaOH-H_2S, thioacetamide as the source of H_2S), with H_2S concentrations ranging from 0.05 to 20 m. In these works, $Au(HS)_2^-$ was deduced to be the dominant Au complex from analyses of solubility dependence on *pH*, H_2S, and H_2 concentrations. Our solubilities are somewhat higher (on average by 0.5 $\log_{10}m_{Au}$) at high *T* (> 350°C) and low *P* (300 bar) than the values calculated using $Au(HS)_2^-$ stability constants reported by Stefánsson and Seward (2004) and Benning and Seward (1996) from Au solubility measurements in H_2-NaOH-H_2S solutions at lower H_2S concentrations (0.01-0.1m), and by Tagirov et al. (2005, 2006) from solubility experiments with the pyrite-pyrrhotite-magnetite mineral assemblage (~0.01-0.2m H_2S). Nevertheless, given the large experimental and computational uncertainties intrinsic at temperatures above 400°C (see Appendix), our solubilities are not meaningfully distinguishable from those datasets. Similarly, our solubilities are ~0.8 log unit higher than those calculated at

300 and 350°C from $Au(HS)_2^-$ stability constants of Pan and Wood (1994) who studied Au solubility in $NaHS-Na_2SO_4$ solutions, but high uncertainties reported for their stability constants do not allow definitive conclusions. Finally, our spectroscopically measured solubilities are in surprisingly good agreement with the first HKF model predictions of Sverjensky et al. (1997) for the $Au(HS)_2^-$ complex, and in reasonable agreement (within 0.2-0.8 log unit) with the theoretical revision of Akinfiev et al. (2008) that included recent solubility data on $Au(HS)_2^-$ (Stefánsson and Seward, 2004; Tagirov et al., 2005, 2006). In contrast to the above studies, our XAFS solubility data are in marked disagreement with the results of Loucks and Mavrogenes (1999) on Au solubility at 500-700°C and 1-4 kbar, which suggest the formation of the neutral tetrakis(hydrogensulfide) species $AuHS(H_2S)_3^0$. The HKF equation-of-state coefficients for this complex reported in the above study yield gold solubilities at $T \leq$ 350°C up to 0.8-1.0 log unit higher than those measured in the present work at neutral *pH* in the $Au(HS)_2^-$ stability domain ($5 \leq pH \leq 8$). At the same time, at higher T in low-H_2S experiments (400-450°C, exp #3 and 4), the thermodynamic model of Loucks and Mavrogenes (1999) yields Au solubilities an order of magnitude lower than those measured by XAFS in our study, suggesting that this species is negligible in near-neutral solutions at low m_S and high T.

Thus, with the only exception of the latter study, our XAFS-derived solubilities are in reasonable agreement with the majority of measurements in batch and flow-through reactors, indicating that $Au(HS)_2^-$ is by far the dominant Au species at neutral to slightly basic *pH* over a wide range of T and m_S to at least 450°C. The formation constants of $Au(HS)_2^-$, derived in this study based on the XAFS-measured Au solubilities and the sulfur aqueous speciation calculated using available thermodynamic data (see Appendix and Table A1) are reported in Table 5. They are identical within errors with those from the majority of experimental and theoretical studies carried out over the last 20 years.

4.2.2. H_2O-S (-Na_2SO_4-H_2SO_4) solutions at acidic pH (1.5-5.0)

Despite the large scatter of Au concentrations measured in the S-H_2O experiments at acidic *pH* (Fig. 7a), they are systematically higher, by at least one log unit, than those predicted using the HKF parameters for the $AuHS^0$ species recommended by Akinfiev et al. (2008) based on the analysis of gold solubility studies of Gibert et al. (1998), Baranova and Zotov (1998), Stefánsson and Seward (2004), and Tagirov et al. (2005, 2006), conducted in acidic solutions using a variety of techniques and H_2S sources (e.g., S-Na_2SO_4, H_2-H_2S-NaOH, sulfide and silicate mineral assemblages, thioacetamide, see Table A2 for details). The XAFS-derived Au solubilities are 1-2 log units higher than those predicted from those solubility data at low H_2S concentrations. These studies suggest $AuHS^0$ to be the dominant Au complex, and $Au(HS)_2^-$ to be minor at acidic conditions (< 10% of total Au at *pH*<4). In contrast, our dissolved Au concentrations at 300°C are comparable to those predicted from Au solubility measurements in thioacetamide solutions by Dadze et al. (2000) who tentatively interpreted their data at acidic *pH* by the formation of the $AuHS^0$ complex. However, large uncertainties intrinsic to the use of thioacetamide as the source of H_2S and H_2 by these authors hamper quantitative comparisons. Consequently, Dadze at al. (2000) data were not considered when comparing XAFS measurements at acidic *pH* with $AuHS^0$ concentration predictions from the literature (Fig. 7). Thus, the high solubilities measured by XAFS in acidic solutions, together with EXAFS and XANES structural data in favor of an AuS_2 stoichiometry, contradict the dominant presence of $AuHS^0$ suggested in the studies discussed above.

The steady-state Au concentrations, measured *in H_2O-S-Na_2SO_4 solutions (exp # 9 and 10) at pH between 4 and 5*, at 400°C are in reasonable agreement, within 0.3 log unit, with those derived using the stability constants for $AuHS^0$ and $Au(HS)_2^-$ from solubility studies of Shenberger and Barnes (1989), Dadze et al. (2000), Fleet and Knipe (2000), Stefánsson and Seward (2004), Tagirov et al. (2005), and the theoretical work of Sverjensky et al. (1997) and

Akinfiev et al. (2008). The stability constants of $AuHS^0$ reported by Gibert et al. (1998) from solubility measurements at *pH* 4-5 yield calculated Au concentrations an order of magnitude lower, which is likely due to underestimation of the $Au(HS)_2^-$ contribution in their data analysis. At 300°C, the solubility measured in this study is systematically higher, by a factor of 5 to 15, than the available literature values, with the only exception of those of Dadze at al. (2000) that display a decent agreement. Note that according to most studies cited above (except Gibert et al., 1998), $Au(HS)_2^-$ should represent between 70 and 95% of total Au at our experimental conditions in the *pH* range 4-5 at 300°C (Fig. 2). Thus, similarly to the more acidic solutions discussed above, our experiments further confirm the presence, in addition to $AuHS^0$ and $Au(HS)_2^-$, of other Au-S complexes in the intermediate *pH* range ($4 \leq pH \leq 5$), at least at 300°C.

Among these species, the $Au(H_2S)HS^0$ complex might be a good candidate, which was suggested by Hayachi and Ohmoto (1991) from Au solubility measurements in H_2O-S-Na_2SO_4 solutions similar to those used in our work. This species matches well both the two-fold stoichiometry and measured solubilities in our solutions at $pH \leq 5$. Despite potentially large uncertainties related to the derivation of the species stoichiometry from their study and extrapolation of the reported stability constants to temperatures above 350°C, their data yield Au solubilities in fair agreement with our results, within $\leq$ 0.3 log units (Table A2). The solubilities measured in this study in the 300-400°C range are also in reasonable agreement (± 0.5 log m_{Au}) with those calculated using the $Au(H_2S)HS^0$ stability constants reported by Wood et al. (1987), who assumed the dominant formation of this species in acidic Cl-free solutions equilibrated with sulfide mineral assemblages. Our derived stability constants for this complex (Table 5), using the calculated concentrations of H_2S and H_2 from Table A1, are the same within errors as those reported in both works cited above. Calculations using our values together with those for $Au(HS)_2^-$ from Table 5 indicate that $Au(H_2S)HS^0$ is the dominant

species at *pH*<3 corresponding to S-H_2O(-H_2SO_4) solutions of this study, but negligible at *pH*>6 in S-H_2O-NaOH solutions, and both species form in comparable amounts at intermediate *pH* of 4-5 in S-H_2O-Na_2SO_4 solutions. This speciation scheme is in line with both the evolution of Au solubilities and XAFS features as a function of *pH* (see above).

Our measured solubilities at *pH*≤~5 do not support the presence of the neutral $AuHS(H_2S)_3^0$ complex suggested by Loucks and Mavrogenes (1999). Calculations using the HKF parameters of this species reported by these authors yield solubilities two orders of magnitude higher than those we measured in the S-H_2O(-Na_2SO_4-H_2SO_4) system. Unfortunately, the formation in S-bearing acidic solutions of other Au complexes with sulfite, thiosulfate or polysulfide ligands, which match the XAFS structural data (see section 4.1), cannot be tested rigorously using our solubility results because of the lack of stability data for such Au complexes and for those sulfur forms at super-ambient conditions. Tentative values of stability constants estimated in this study for the mixed $Au(HS)SO_2^0$ complex assuming its predominance in S-H_2O(-H_2SO_4) experiments (Table 5) indicate that its amount is controlled by SO_2 concentration which decreases rapidly with increasing *pH* (Fig. 2, Table A1). This species, if it forms, is thus not able to account alone for the elevated Au solubilities in the moderately acidic *pH* range (~4-5), thus suggesting formation of additional Au complexes.

Thiosulfate and polysulfides may also form as intermediate species during sulfur dissolution and hydrolysis; thiosulfate species have been proposed to mediate redox reactions between sulfide and sulfate in hydrothermal solutions (e.g., Ohmoto and Lasaga, 1982). Such S species formed during initial sulfur dissolution/oxidation steps may contribute further to the Au^I complexing. The large scatter of Au dissolved concentrations in the H_2O-S solutions observed at moderate *T* (300°C), and the irregular Au concentration evolution with time in the H_2O-S-Na_2SO_4 experiments (e.g., Fig. 7) might indeed reflect transient, metastable formation of such intermediate sulfur species, particularly during the initial steps of sulfur dissolution, followed

by the decrease of their concentrations when the system evolves towards equilibrium with increasing *T* and run duration.

5. GEOLOGICAL IMPLICATIONS

5.1. Gold hydrogensulfide complexes in hydrothermal systems

To our knowledge, this report provides the first in situ spectroscopic data on the identity and stability of aqueous gold sulfur-bearing complexes likely responsible for the gold transport and distribution in the majority of epithermal and porphyry-style deposits as well as in active geothermal-volcanic fields. In particular, this study provides the first direct spectroscopic characterization of the $Au(HS)_2^-$ complex dominant in near-neutral fluids over a wide range of sulfur concentrations. Gold solubilities in near-neutral sulfur-bearing aqueous solutions measured using in situ XAFS spectroscopy are in good agreement with the majority of data sources for $Au(HS)_2^-$ stability constants reported in the literature based exclusively on ex situ solubility measurements. These and our data leave little doubt that this species is by far the dominant Au-bearing complex in a wide range of conditions corresponding to hydrothermal ore-forming fluids and geothermal waters at circa-neutral *pH*.

Both the results obtained in this study and existing data show that the stability domain of this negatively charged hydrogensulfide complex, and thus the overall gold solubility, decrease with decreasing *pH*, so that this species becomes negligible in acidic high-*T* fluids and vapors owing to the increasing stability of neutral species and decreasing amounts of anionic ligands (HS^-). However, our structural and solubility data obtained in acidic H_2O-S-Na_2SO_4-H_2SO_4 model solutions ($pH \leq 5$) contradict the dominant formation of the neutral hydrogensulfide species $AuHS^0$ proposed in many solubility studies. The EXAFS structural parameters, very similar to those derived for $Au(HS)_2^-$, together with quantum-chemical

calculations of species structures and measured Au solubilities, rather suggest the formation of neutral bisulfide complexes, most likely $AuHS(H_2S)^0$, in acid S-rich ($m_{H_2S} \geq 0.1$m) solutions. Note also that from the point of view of the hard-soft complexation rules, one does not expect
595 significant formation of mixed-ligand complexes with constituting ligands of quite different hardness (Crerar et al., 1985). Indeed, the stoichiometry $(H_2O)Au(SH)$ for the uncharged hydrogensulfide species, imposed by the Au^I coordination chemistry and supported by quantum chemical calculations of this study, implies the presence of a moderately hard (H_2O) and a very soft (HS) ligand bound to the soft Au^+ cation in the same complex. The elevated sulfide
600 concentrations (up to few wt%) typical of magmatic-hydrothermal fluids would favor the substitution of the water molecule in the $(H_2O)Au(HS)^0$ complex by a much softer H_2S ligand; this is also in accordance with the general complexation rules (e.g., Brimhall and Crerar, 1987; Cotton and Wilkinson, 1988).

The neutral bis(hydrogensulfide) complex $AuHS(H_2S)^0$ may thus be responsible for
605 enhanced Au partitioning into the low-density vapor phase, in comparison to the coexisting salt-rich brine, observed in laboratory experiments at acidic conditions (Pokrovski et al., 2008a) and natural fluid inclusions from porphyry deposits (e.g., Heinrich, 2007; references therein). The small dipole moment and very weak solvation by outer-sphere water molecules of this species and, by inference, of analogous Cu and Pt species, may greatly favor the solubility of
610 these chalcophile metals in S-rich low-density vapor phase as observed both in nature and experiments (e.g., Pokrovski et al., 2005b, 2008a).

5.2. Effect of S ligands other than sulfide on Au transport

Although, at the present state of our knowledge, the neutral bis(hydrogensulfide)
615 complex seems to be the best candidate to describe the Au speciation in the S-rich acidic solutions examined in this study, the presence of thiosulfate and polysulfide complexes in

solutions saturated with elemental sulfur might also account for the measured solubilities and [S-Au-S] stoichiometries. The stability of $Au(S_2O_3)_2^{3-}$ is comparable to that for $Au(HS)_2^-$ at ambient conditions ($\log_{10}\beta$ for both species ~ 28-30, Seward, 1989; Stefánsson and Seward, 2004). According to Webster (1986), the thiosulfate complex may be responsible for the gold remobilization during low-temperature oxidation of sulfide ores. By analogy with the Au hydrogensulfide complexes, more protonated and less charged Au-thiosulfate species are expected to form at acidic *pH*. Polysulfide Au complexes were reported to form at moderate temperatures (< 150°C) in solutions saturated with elemental sulfur; they were suggested to play a role in Au transport in near-surface epithermal settings and active geothermal fields (Berndt et al., 1994). For example, thiosulfate concentrations in some geothermal springs at $T \leq 100$°C attain values comparable to those of H_2S, and thus may efficiently complex Au and similar metals (Migdisov and Bychkov, 1998; Xu et al., 1998; references therein). Estimation of the impact of such ligands on Au transport by hydrothermal fluids is greatly hampered by the lack of data on the stability and amounts of these sulfur forms at above-ambient temperatures and pressures. For example, recent measurements by Raman spectroscopy in a hydrothermal diamond-anvil cell on H_2O-S(-NaOH) solutions at very high *P* (10-40 kbar) and moderate *T* (200-300°C) indicate the dominant formation of polysulfide (e.g., $H_{0-2}S_3$) and/or polythionate (e.g., $H_{0-2}S_2O_5$) species (Pokrovski and Dubrovinsky, 2009), in marked contrast with thermodynamic predictions based on low *T*-*P* data of sulfide and sulfate as the major forms in solution (Fig. 2).

Another important sulfur ligand that may impact the gold transport in high-*T* magmatic-hydrothermal fluids is sulfite (SO_2, and its dissociation products, HSO_3^- and SO_3^{2-}). Gold-sulfite species may account for the observed Au two-fold S coordination and elevated solubilities in comparison to $AuHS^0$. Because metal-ligand interactions generally become 'harder' with increasing temperature, following the decrease of the solvent dielectric constant

and thus reinforcement of the coulombic attraction (e.g., Crerar et al., 1985), high-temperature conditions might be beneficial for Au complexing with SO_2 which is a "harder" ligand than H_2S. The formation of such species is thus expected to be strongly favored in magmatic fluids and gases typical of active convergent margins where SO_2 often largely dominates over H_2S (e.g., Borisova et al., 2006). The geological spatial and temporal links, widely documented in these areas between magmatic plutons and overlaid epithermal high sulfidation Au-Cu deposits, are often interpreted by the transport of Au and Cu by oxidizing, acidic, magmatic vapor phases enriched in SO_2 (e.g., Hedenquist and Lowenstern, 1994; Heinrich, 2007; Pokrovski et al., 2008a). Like for other sulfur species of intermediate valences, the major obstacle in quantifying the contribution of SO_2 in Au transport is the paucity of high *T-P* thermodynamic and *PVTX* data for S^{IV} gaseous and aqueous species and their partitioning between vapor, brine and silicate melt. For example, the available thermodynamic properties of aqueous SO_2 and its dissociation products used in modeling of the sulfur speciation at hydrothermal-magmatic conditions are based on extrapolations from measurements performed at $T \leq 110$°C (Shock et al., 1989; Schulte et al., 2001). This may induce uncertainties of several 10's of kJ/mol in the estimation of the Gibbs free energy of SO_2(aq) and corresponding sulfite anions at $T \geq$ 300-400°C. Such uncertainties may yield orders-of-magnitude variations in the calculated amounts of sulfite sulfur and its anions in aqueous solution (depending of the chemical composition). One of the major near-future challenges in the hydrothermal research will be to assess the identity and amounts of the different complexes formed by sulfur in aqueous fluid and vapor phase, in particular using in situ spectroscopic methods, both in model laboratory systems and natural fluid and melt inclusions.

6. CONCLUDING REMARKS

This report is the first measurement, to our knowledge, that uses in situ XAFS spectroscopy to determine the stability and structure of Au^{I} sulfur-bearing complexes in S-rich fluids pertinent to hydrothermal-magmatic gold ore deposits. The combination of XAFS spectra analyses with quantum chemical calculations of structures of Au-S aqueous complexes and in situ solubility measurements provides new information about the identities, structures and stabilities of major Au-S species operating in high *T*-*P* natural fluids.

The new spectroscopic characterization of the $Au(HS)_2^-$ complex dominant in near-neutral fluids over a wide range of sulfur concentrations and *T*-*P* parameters is in agreement with most previous solubility work. In this species, Au is bound to two sulfur atoms in a linear geometry, with Au-S distances of 2.29±0.01 Å typical for the crystal chemistry of Au^{I} sulfide-bearing compounds.

In acidic solutions, the Au atomic environment obtained from XAFS spectra is very similar to that in neutral solutions. These findings, together with measured high Au solubilities, are inconsistent with the predominance of the gold hydrogensulfide complex $Au(HS)^0$ suggested by solubility studies. Our structural and solubility results imply the dominant formation of other species in which Au is coordinated with 2 sulfur atoms, such as the $AuHS(H_2S)^0$ complex suggested in some solubility studies. This species may account for the elevated Au solubilities in acidic fluids and vapors and enhanced vapor-brine partitioning of Au at H_2S concentrations higher than ~0.1 m, as found in recent experimental and natural fluid inclusions studies.

However, because of the complex sulfur speciation in acidic solutions that involves sulfite, thiosulfate and polysulfide species, the formation of Au^{I} complexes with these sulfur ligands (e.g., $AuHS(SO_2)^0$, $Au(H_mS_2O_3)_2^{2-m}$, $Au(H_mS_n)_2^{2-m}$) cannot be ruled out. The major obstacle in the quantifying of the contribution of such species to the Au speciation is the insufficient knowledge of the aqueous speciation of sulfur itself at elevated *T*-*P*.

Systematic studies of the identity, structure and stability of the different species of sulfur in aqueous fluid and vapor phase are thus urgently needed to quantitatively assess the effect of the different sulfur forms on the fate of gold and other chalcophile metals in hydrothermal-magmatic environments.

Acknowledgements: This work was supported by CNRS grants from the French GDR Transmet and 3F (Fluides-Failles-Flux) programs, a PHC linkage grant (LMTG-ETH), and by funding from the Laboratoire Européen Associé Géochimie Environnementale (LEAGE). We are grateful to the ESRF and French CRG Committees for providing beam time and access to the synchrotron facility. We are indebted to Olivier Geaymond and Eric Lahera for their help in the X-ray cell installation and running, and Rémi Bruyère and Alain Prat for the helium pressure regulation system. Bruce Ravel is thanked for his advice on the HORAE software, François Farges for discussions on Au XAFS spectroscopy, and Nikolay Akinfiev for a thermodynamic feedback. Richard Bryce and John Charnock are acknowledged for providing their gold-thiosulfate spectra for comparison. The English of the article has been improved by efforts of Chris Pearce. Editorial handling of Jim Kubicki and constructive comments of two anonymous referees are greatly appreciated.

References

Akinfiev N.N. and Diamond L.W. (2003) Thermodynamic denscription of aqueous nonelectrolytes at infinite dilution over a wide range of state parameters. *Geochim. Cosmochim. Acta* **67**, 613-627.

Akinfiev N.N. and Zotov A.V. (2001) Thermodynamic description of chloride, hydrosulphide, and hydroxide complexes of Ag(I), Cu(I), and Au(I) at temperatures of 25-500°C and pressures of 1-2000 bar. *Geochem. Intern.* **39** (10), 990-1006.

Akinfiev N.N., Baranova N.N., Zotov A.V. and Tagirov B.R. (2008) Thermodynamic description of aqueous components in the system Cu-Ag-Au-S-Se-O-H in the range of temperatures 0-600°C and pressures 1-3000 bars. In *Experimental studies of endogenic processes* (eds. I. D. Ryabchikov, Yu. B. Shapovalov, E. G. Osadchii). Publishing Office of the Institute of the Problems of Chemical Physics, Chernogolovka, Russia, pp. 184-203 (in Russian).

Bakker R.J. (2003) Package FLUIDS 1. Computer programs for analysis of fluid inclusion data and for modelling bulk fluid properties. *Chem. Geol*. **194**, 3-23.

Baranova N.N. and Zotov A.V. (1998) Stability of gold sulfide species ($AuHS°_{(aq)}$ and $Au(HS)_2^-{}_{(aq)}$) at 300, 350°C and 500 bar: experimental study. *Min. Mag.* **62A**, 116-117.

Becke A. D. (1993) Density-functional thermochemistry. III. The role of exact exchange. *J. Chem. Phys.* **98**, 5648-5652.

Benfield R.E., Filipponi A., Bowron D.T., Newport R.J. and Gurman S.J. (1994) An x-ray absorption study of gold coordination compounds: EXAFS refinements and double-electron excitation background. *J. Phys.: Condens. Matter* **6**, 8449-8468.

Benning L.G. and Seward T.M (1996) Hydrosulphide complexing of Au (I) in hydrothermal solutions from 150–400°C and 500–1500 bar. *Geochim. Cosmochim. Acta* **60**, 1849-1871.

Berndt M.E., Buttram T., Earley D., III, and Seyfried W.E. (1994) The stability of gold polysulfide complexes in aqueous sulfide solutions: 100 to 150°C and 100 bars. *Geochim. Cosmochim. Acta* **58**, 587-594.

Bishop P., Marsh P., Brisdon A.K., Brisdon B.J., Mahon M.F. (1998) X-ray crystallographic and extended X-ray absorption fine structure studies of gold(I) complexes containing weak intermolecular interactions. *J. Chem. Soc. Dalton Trans.* **4**, 675-682.

Bondarenko G.V. and Gorbaty Y.E. (1997) In situ Raman spectroscopic study of sulfur-saturated water at 1000 bar between 200 and 500°C. *Geochim. Cosmochim. Acta* **61**, 1413-1420.

Borisova A.Yu., Pichavant M., Bény J.-M., Rouer O. and Pronost J. (2005). Constraints on dacite magma degassing and regime of the June 15, 1991, climactic eruption of Mount Pinatubo (Philippines): New data on melt and crystal inclusions in quartz. *J. Volcan. Geotherm. Res.* **145**, 35-67.

Borisova A.Yu., Pichavant M., Polvé M., Wiedenbeck M., Freydier R. and Candaudap F. (2006). Trace element geochemistry of the 1991 Mt. Pinatubo silicic melts, Philippines: Implications for ore-forming potential of adakitic magmatism. *Geochim. Cosmochim. Acta* **70**, 3702-3716.

Brimhall G.H. and Crerar D.A. (1987) Ore fluids: magmatic to supergene. *Rev. Miner*. **17**, 235-321.

Bryce R.A., Charnock J.M., Pattrick R.A.D. and Lennie A.R. (2003) EXAFS and density functional study of gold(I) thiosulfate complex in aqueous solution. *J. Phys. Chem.* **A 107**, 2516-2523.

Chase M.W., Jr. (1998) NIST-JANAF Thermochemical Tables, Forth Edition. *J. Phys. Chem. Ref. Data,* Monograph No. 9.

Cotton A.F. and Wilkinson G. (1988) *Advanced Inorganic Chemistry*. Fifth Edition, Wiley.

Dadze T. P., Kashirtseva G. A. and Ryzhenko B. N. (2000) Gold solubility and species in aqueous sulfide solutions at T=300°C. *Geochem. Intern.* **38,** 708-712.

Elam W.T., Ravel B.D. and Sieber J.R. (2002) A new atomic database for X-ray spectroscopic calculations. *Radiat. Phys. Chem*. **63**, 121-128.

Elder R.C. and Eidsness M.K. (1987) Synchrotron X-ray studies of metal-based drugs and metabolites. *Chem. Rev.* **87**, 1027-1046.

Ellis A.J. and Giggenbach W. (1971) Hydrogen sulphide ionization and sulphur hydrolysis in high-temperature solution. *Geochim. Cosmochim. Acta* **35**, 247-260.

Feller D., Glendening E. D. and Jong, W. A. (1999) Structures and binding enthalpies of $M^+(H_2O)_n$ clusters, M=Cu, Ag, Au. *J. Chem. Phys*. **110**, 1475-1491.

Fleet M.E. and Knipe S.W. (2000) Solubility of native gold in H-O-S fluids at 100-400°C and high H_2S content. *J. Solution Chem*. **29**, 1143-1157.

Frisch M.J., Trucks G.W., Schlegel H.B., Scuseria G.E., Robb M.A., Cheeseman J.R., Montgomery, Jr. J.A., Vreven T., Kudin K.N., Burant J.C., Millam J.M., Iyengar S.S., Tomasi J., Barone V., Mennucci B., Cossi M., Scalmani G., Rega N., Petersson G.A., Nakatsuji H., Hada M., Ehara M., Toyota K., Fukuda R., Hasegawa J., Ishida M., Nakajima T., Honda Y., Kitao O., Nakai H., Klene M., Li X., Knox J.E., Hratchian H.P., Cross J.B., Bakken V., Adamo C., Jaramillo J., Gomperts R., Stratmann R.E., Yazyev O., Austin A.J., Cammi R., Pomelli C., Ochterski J.W., Ayala P.Y., Morokuma K., Voth G.A., Salvador P., Dannenberg J.J., Zakrzewski V.G., Dapprich S., Daniels A.D., Strain M.C., Farkas O., Malick D.K., Rabuck A.D., Raghavachari K., Foresman J.B., Ortiz J.V., Cui Q., Baboul A.G., Clifford S., Cioslowski J., Stefanov B.B., Liu G., Liashenko A., Piskorz P., Komaromi I., Martin R.L., Fox D.J., Keith T., Al-Laham M.A., Peng C.Y., Nanayakkara A., Challacombe M., Gill P.M.W., Johnson B., Chen W., Wong M.W., Gonzalez C., and Pople J.A. (2004) *Gaussian 03*. Revision C.02, Gaussian, Inc., Wallingford CT.

Gibert F., Pascal M.L. and Pichavant M. (1998) Gold solubility and speciation in hydrothermal solutions: Experimental study of the stability of hydrosulfide complex of gold ($AuHS^0$) at 350 to 450°C and 500 bars. *Geochim. Cosmochim. Acta* **62**, 2931-2947.

Gurevich V.M., Gavrichev K.S., Gorbunov V.E., Baranova N.N., Tagirov B.R., Golushina L.N., Polyakov V.B. (2004) The heat capacity of Au_2S(cr) at low temperatures and derived thermodynamic functions. *Thermochim. Acta* **412**, 85–90.

Hayashi K.I. and Ohmoto H. (1991) Solubility of gold in NaCl- and H_2S-bearing aqueous solutions at 250-350°C. *Geochim. Cosmochim. Acta* **55**, 2111-2126.

Hedenquist J. W. and Lowenstern J. B. (1994) The role of magmas in the formation of hydrothermal ore deposits. *Nature* **370**, 519-527.

Heinrich C.A. (2007) Fluid-fluid interactions in magmatic-hydrothermal ore formation. *Rev. Miner. Geochem.* **65**, 363-387.

Helgeson H.C. and Kirkham D.H. (1974) Theoretical prediction of the thermodynamic behavior of aqueous electrolytes at high pressures and temperatures: II. Debye-Hückel parameters for activity coefficients and relative partial molal properties. *Amer. J. Sci*. **274**, 1199-1261.

Ho P.C., Palmer D.A., and Mesmer R.E. (1994) Electrical conductivity measurements of aqueous sodium chloride solutions to 600°C and 300 MPa. *J. Solution Chem.* **23,** 997-1018.

Ishikawa K., Isonage T., Wakita S. and Suzuki Y. (1995) Structure and electrical properties of Au_2S. *Solid State Ionics* **79**, 60-66.

Johnson J.W., Oelkers E.H. and Helgeson H.C. (1992) SUPCRT92: A software package for calculating the standard molal thermodynamic properties of minerals, gases, aqueous species, and reactions from 1 to 5000 bar and 0 to 1000°C. *Computers & Geosci.* **18**, 899-947; http://geopig.asu.edu/index.html#.

Lengke M. and Southam G. (2006) Bioaccumulation of gold by sulfate-reducing bacteria cultured in the presence of gold(I)-thiosulfate complex. *Geochim. Cosmochim. Acta* **70**, 3646-3661.

Loucks R. R. and Mavrogenes J. A. (1999) Gold solubility in supercritical hydrothermal brines measured in synthetic fluid inclusions. *Science* **284**, 2159-2163.

Migdisov A.A. and Bychkov A. Yu. (1998) The behaviour of metals and sulphur during the formation of hydrothermal mercury-antimony-arsenic minerasization, Uzon caldera, Kamchatka, Russia. *J. Volcanol. Geotherm. Res.* **84**, 153-171.

Newville M. (2001) IFEFFIT: interactive XAFS analysis and FEFF fitting. *J. Synchrotron Rad*. **8**, 322-324.

Oelkers E.H. and Helgeson H.C. (1990) Triple-ion anions and polynuclear complexing in supercritical electrolyte solutions. *Geochim. Cosmochim. Acta* **54**, 727-738.

Ohmoto H. and Lasaga A.C. (1982) Kinetics of reactions between aqueous sulfates and sulfides in hydrothermal systems. *Geochim. Cosmochim. Acta* **46**, 1727-1745.

Pan P. and Wood S.A. (1994) Solubility of Pt and Pd sulfides and Au metal in aqueous bisulfide solutions. II. Results at 200° to 350°C and saturated vapor pressure. *Miner. Deposita* **29**, 373-390.

Pokrovski G.S., Schott J. and Sergeyev A.S. (1995) Experimental determination of the stability constants of $NaSO_4^-$ and $NaB(OH)_4^0$ in hydrothermal solutions using a new sodium selective glass electrode. Implications for boron isotopic fractionation. *Chem. Geol.* **124**, 253-265.

Pokrovski G.S., Roux J., Hazemann J.-L. and Testemale D. (2005a) An X-ray absorption spectroscopy study of argutite solubility and germanium aqueous speciation in hydrothermal fluids to 500°C and 400 bar. *Chem. Geol.* **217**, 127-145.

Pokrovski G.S., Roux J. and Harrichoury J.-C. (2005b). Fluid density control on vapor-liquid partitioning of metals in hydrothermal systems. Geology **33**, 657-660.

Pokrovski G.S., Borisova A.Yu., Roux J., Hazemann J.-L., Petdang A., Tella M. and Testemale D. (2006). Antimony speciation in saline hydrothermal fluids: A combined X-ray absorption fine structure and solubility study. *Geochim. Cosmochim Acta* **70**, 4196-4214.

Pokrovski G.S., Borisova A.Yu. and Harrichoury J.-C. (2008a). The effect of sulfur on vapor-liquid fractionation of metals in hydrothermal systems. *Earth Planet. Sci. Lett*. **266**, 345-362.

Pokrovski G.S., Roux J., Hazemann J.-L., Borisova A.Yu., Gonchar A.A. and Lemeshko M.P. (2008b) In situ X-ray absorption spectroscopy measurement of vapor-brine fractionation of antimony at hydrothermal conditions. *Min. Mag.* **72**, 667-681.

Pokrovski G.S., Tagirov B.R., Schott J., Bazarkina E.F., Hazemann J.-L. and Proux O. (2009) An in situ X-ray absorption spectroscopy study of gold-chloride complexing in hydrothermal fluids. *Chem. Geol*. **259**, 17-29.

Pokrovski G.S. and Dubrovinsky L.A. (2009) Sulfur speciation in aqueous solution and its consequences for metal transport by hydrothermal fluids. *Geochim. Cosmochim. Acta* **73** (in press).

Proux O., Biquard X., Lahera E., Menthonnex J.-J., Prat A., Ulrich O., Soldo Y., Trevisson P., Kapoujyan G., Perroux G., Taunier P., Grand D., Jeantet P., Deleglise M., Roux J.-P. and Hazemann J.-L. (2005) FAME: a new beamline for X-ray absorption investigations of very diluted systems of environmental, material and biological interests. *Phys. Scripta* **T115**, 970-973.

Proux O., Nassif V., Prat A., Ulrich O., Lahera E., Biquard X., Menthonnex J.-J. and Hazemann J.-L. (2006) Feedback system of a liquid-nitrogen-cooled double-crystal monochromator: design and performances. *J. Synchrotron Rad*. **13**, 59-68.

Ravel B. and Newville M. (2005) ATHENA, ARTEMIS, HEPHAESTUS: data analysis for X-ray absorption spectroscopy using IFEFFIT. *J. Synchrotron Rad*. **12**, 537-541.

Robie R.A. and Hemingway B.S. (1995) Thermodynamic properties of minerals and related substances at 298.15 K and 1 bar (10^5 pascals) pressure and at higher temperatures. *U.S. Geol. Survey Bull*. **2131**.

Robinson B.W. (1973) Sulphur isotope equilibrium during sulphur hydrolysis at high temperatures. *Earth Planet. Sci. Lett.* **18**, 443-450.

Ruben H., Zalkin A., Faltens M.O. and Templeton D.H. (1974) Crystal structure of soldium gold(I) thiosulfate dihydrate, $Na_3Au(S_2O_3)_2{\cdot}2H_2O$. *Inorg. Chem*. **13**, 1836-1839.

Sayers D.E. (2000) Report of the International XAFS Society Standards and Criteria Commitee. http://www.i-x-s.org/OLD/subcommittee_reports/sc/.

Schulte M.D., Shock E.L. and Wood R.H. (2001) The temperature dependence of the standard-state thermodynamic properties of aqueous nonelectrolytes. *Geochim. Cosmochim. Acta* **65**, 3919-3930.

Schwerdtfeger P., Dolg M., Schwarz W. H. E., Bowmaker G. A., Boyd P. D. W. (1989) Relativistic effects in gold chemistry. I. Diatomic gold compounds. *J. Chem. Phys*. **91**, 1762-1774.

Skibsted L. H. and Bjerrum J. (1977) Studies on gold complexes. III. The standard electrode potentials of aqua gold ions. *Acta Chem. Scand. A* **31,** 155-156.

Seward T.M. (1973) Thio complexes of gold and the transport of gold in hydrothermal ore solutions. *Geochim. Cosmochim Acta* **37**, 379-399.

Seward T.M. (1989) The hydrothermal chemistry of gold and its implications for ore formation: Boiling and conductive cooling as examples. *Econ. Geol. Monogr*. **6**, 398-404.

Seward T.M. and Driesner T. (2004). Hydrothermal solution structure: experiments and computer simulations, pp. 149-182, in: *Aqueous Systems at Elevated Temperatures and Pressures* (D.A. Palmer, R. Fernandez-Prini, and A.H. Harvey, editors), Elsevier.

Shenberger D.M. and Barnes H.L. (1989) Solubility of gold in aqueous sulfide solutions from 150 to 350°C. *Geochim. Cosmochim. Acta* **53**, 269-278.

Sherman D.M. (2001). Quantum chemistry and classical simulations of metal complexes in aqueous solutions. *Rev. Miner. Geochem*. **42**, 273-317.

Shock E.L., Helgeson H.C., and Sverjensky D.A. (1989) Calculation of the thermodynamic and transport properties of aqueous species at high temperatures and pressures: Standard partial molal properties of inorganic neutral species. *Geochim. Cosmochim. Acta* **53**, 2157-2183.

Shock E.L., Oelkers E.H., Johnson J.W., Sverjensky D.A. and Helgeson H.C. (1992) Calculation of the thermodynamic properties of aqueous species at high pressures and temperatures. *J. Chem. Soc. Faraday Trans*. **88**, 803-826.

Shock E.L., Sassani D.C., Willis M., and Sverjensky D.A. (1997) Inorganic species in geologic fluids: Correlations among standard molal thermodynamic properies of aqueous ions and hydroxide complexes. *Geochim. Cosmochim. Acta* **61,** 907-950.

Shvarov Yu.V. (1999) Algorithmization of the numeric equilibrium modelling of dynamic geochemical processes. *Geochem. Intern.* **37,** 571-576; http://www.geol.msu.ru/deps/geochems/soft/index.html.

Sorokin V.I. and Dadze T.P. (1994) Solubility and complex formation in the systems Hg-H_2O, S-H_2O, SiO_2-H_2O and SnO_2-H_2O, in: Shmulovich, K.I, Yardley, B.W.D., Gonchar, G.G. (Eds.), *Fluids in the Crust: Equilibrium and Transport Properties*, Chapman & Hall, London, pp. 57-93.

Stefánsson A. and Seward T.M. (2004). Gold(I) complexing in aqueous sulphide solutions to 500°C at 500 bar. *Geochim. Cosmochim. Acta* **68**, 4121-4143.

Takano Yu. and Houk K.N. (2005) Benchmarking of the conductor-like polarizable continuum model (CPCM) for aqueous solvation free energies of neutral and ionic organic molecules. *J. Chem. Theory Comput.* **1,** 70-77.

Tagirov B.R., Salvi S., Schott J. and Baranova N.N. (2005). Experimental study of gold-hydrosulphide complexing in aqueous solutions at 350-500°C, 500 and 1000 bars using mineral buffers. *Geochim. Cosmochim. Acta* **69**, 2119-2132.

Tagirov B.R., Baranova N.N., Zotov A.V., Schott J. and Bannykh L.N. (2006). Experimental determination of the stabilities Au_2S(cr) at 25 °C and $Au(HS)_2^-$ at 25-250°C. *Geochim. Cosmochim. Acta* **70**, 3689-3701.

Tella M. and Pokrovski G.S. (2009) Antimony(III) complexing with O-bearing organic ligands in aqueous solution: An X-ray absorption fine structure spectroscopy and solubility study. *Geochimica et Cosmochimica Acta* **73**, 268-290.

Teo B.K. (1986) *EXAFS: Basic Principles and Data Analysis*. Springer-Verlag.

Testemale D., Hazemann J.-L., Pokrovski G.S., Joly Y., Roux J., Argoud R. and Geaymond O. (2004) Structural and electronic evolution of the $As(OH)_3$ molecule in high temperature aqueous solutions: An x-ray absorption investigation. *J. Chem. Phys.* **121,** 8973-8982.

Testemale D., Argoud R., Geaymond O. and Hazemann J.-L. (2005). High pressure/high temperature cell for x-ray absorption and scattering techniques. *Rev. Sci. Instrum*. **76**, 043905-043909.

Tossel J.A. (1996) The speciation of gold in aqueous solution: A theoretical study. *Geochim. Cosmochim. Acta* **60**, 17-29.

Wallace P.J. (2001) Volcanic SO_2 emissions and the abundance and distribution of exsolved gas in magma bodies. *J. Volcanol. Geotherm. Res*. **108**, 85-106.

Webster J.G. (1986) The solubility of gold and silver in the system Au-Ag-S-O_2-H_2O at 25°C and 1 atm. *Geochim. Cosmochim. Acta* **50**, 1837-1845.

Wood S., Crerar D.A. and Borcsik M.P. (1987) Solubility of the assemblage pyrite-pyrrhotite-magnetite-sphalerite-galena-gold-stibnite-bismuthinite-argentite-molybdenite in H_2O-NaCl-CO_2 solutions from 200 to 350°C. *Econ. Geol*. **82**, 1864-1887.

Xu Y., Schoonen M.A.A., Nordstrom D.K., Cunningham K.M. and Ball J.W. (1998) Sulfur geochemistry of hydrothermal waters in Yellowstone national park: I. The origin of thiosulfate in hot spring waters. *Geochim. Cosmochim. Acta* **62**, 3729-3743.

Zotov N. and Keppler H. (2002) Silica speciation in aqueous fluids at high pressures and temperatures. *Chem. Geol.* **184**, 71-82.

Zotov A.V., Kudrin A.V., Levin K.A., Shikina N.D., and Var'yash L.N. (1995) Experimental studies of the solubility and complexing of selected ore elements (Au, Ag, Cu, Mo, As, Sb, Hg) in aqueous solutions. in: Shmulovich, K.I, Yardley, B.W.D., Gonchar, G.G. (Eds.), *Fluids in the Crust. Equilibrium and Transport Properties*, Chapman & Hall, London, pp. 95-138.

Table 1. Au^{I}-S species geometries (Au-S bond distances are in Å and angles in degrees), calculated using quantum-chemical methods.

Species	Au-SH	Au-SH_2 *or* Au-SO_{2-3}	**Au-S (mean)**	Au-O	<S-Au-S *or* <S-Au-O	Medium	Method [a]
$AuHS(H_2S)^0$, cis	2.283	2.375	**2.33**	NA	177.3	gas	MP2
$AuHS(H_2S)^0$, cis	2.298	2.368	**2.33**	NA	177.5	aq	MP2
$AuHS(H_2S)^0$, trans	2.283	2.375	**2.33**	NA	179.9	gas	MP2
$AuHS(H_2S)^0$, trans	2.299	2.368	**2.33**	NA	179.5	aq	MP2
$AuHS(H_2O)^0$, cis	2.264	NA	**2.26**	2.204	178.3	gas	MP2
$AuHS(H_2O)^0$, cis	2.277	NA	**2.28**	2.151	177.5	aq	MP2
$AuHS(H_2O)^0$, trans	2.264	NA	**2.26**	2.204	178.9	gas	MP2
$AuHS(H_2O)^0$, trans	2.279	NA	**2.28**	2.151	179.6	aq	MP2
$Au(HS)_2^-$	2.336	NA	**2.34**	NA	178.9	gas	MP2
$Au(HS)_2^-$	2.327	NA	**2.33**	NA	178.7	aq	MP2
$Au(HS)_2^-$	2.374	NA	**2.37**	NA	178.9	gas	DFT
$Au(HS)_2^-$	2.365	NA	**2.37**	NA	178.6	aq	DFT
$AuHS(SO_2)^0$	2.270	2.283	**2.28**	NA	178.8	gas	MP2
$AuHS(SO_2)^0$	2.284	2.288	**2.29**	NA	179.0	aq	MP2
$Au(HSO_3)_2^-$	NA	2.325	**2.33**	NA	180.0	gas	MP2
$Au(SO_3)_2^{3-}$	NA	2.387	**2.39**	NA	180.0	gas	MP2
$Au(SO_3)_2^{3-}$	NA	2.322	**2.32**	NA	180.0	aq	MP2

[a] MP2 = MP2/SDD(Au)/6-311++G(p,d)(S,O,H) in gas phase; CPCM/MP2/SDD(Au)/6-311++G(p,d)(S,O,H) in aqueous solution (ε=78.3);
DFT = B3LYP/SDD(Au)/6-311++G(p,d)(S,O,H) in gas phase; CPCM/B3LYP/SDD(Au)/6-311++G(p,d)(S,O,H) in aqueous solution(ε=78.3).
NA = not applicable

Table 2. Gold(I) local structure in aqueous solution in the system $Au_{(s)}$-H_2O-S-NaOH-Na_2SO_4 as a function of temperature and pressure, derived from fitting EXAFS spectra at Au L_3-edge.

T (°C)	atom	N (atoms)	R (Å)	σ^2 (Å^2)	Δe (eV)	P-factor
# 1, 600 bar: 3.48m S-2.17m NaOH						
300	S	2.2	2.292	0.0050	8.5	0.014
# 2, 600 bar: 2.66m S-1.42m NaOH						
300	S	2.2	2.290	0.0040	8.0	0.006
350	S	2.2	2.293	0.0045	8.0	0.009
400	S	2.1	2.292	0.0045	7.9	0.006
450	S	2.1	2.293	0.0048	7.9	0.008
# 3, 600 bar: 0.53m S-0.40m NaOH						
300	S	2.1	2.293	0.0035	8.0	0.004
400	S	2.1	2.297	0.0046	8.1	0.004
450	S	2.1	2.298	0.0050	7.9	0.006
# 4, 300 bar: 0.58m S-0.40m NaOH						
200	S	2.0	2.292	0.0025	7.7	0.006
300	S	2.0	2.293	0.0038	8.4	0.004
400	S	2.1	2.299	0.0052	7.9	0.008
# 5, 600 bar: 1.0m S-H_2O						
300	S	2.1	2.298	0.0034	8.6	0.007
400	S	2.3	2.292	0.0040	8.3	0.016
# 8, 600 bar: 0.8m S-H_2O						
450	S	2.3	2.300	0.0045	9.4	0.017
# 9, 600 bar: 0.51m S-0.55m Na_2SO_4						
300	S	2.2	2.290	0.0038	7.6	0.010
# 10, 600 bar: 0.79m S-0.55m Na_2SO_4						
400	S	2.0	2.290	0.0036	7.7	0.011
Error		±0.2	±0.005	±0.001	±1.5	

R = gold-backscatterer mean distance, N = Au coordination number, σ^2 = squared Debye-Waller factor (relative to $\sigma^2 = 0$ adopted in the calculation of reference amplitude and phase functions by FEFF); Δe = non-structural parameter accounting for phase shift between experimental spectrum and FEFF calculation; P-factor defines goodness of the total fit in R-space as described in FEFFIT (Newville et al., 2001). For all samples the fitted k-and R-ranges were respectively 3.2-10.0 Å^{-1} and 1.3-4.8 Å (not corrected for phase shift). Multiple scattering contributions within the linear S-Au-S' cluster, like Au-S-S'-Au ($R_{ms1} = 2\times R_{Au\text{-}S}$) and Au-S-Au-S'-Au ($R_{ms2} = 2\times R_{Au\text{-}S}$), were included in all fits; their DW factors were found to range between 0.007 and 0.012 Å^2. The number of variables in the fit (N_{var} = 4 to 7) has always been much lower than the number of independent points (N_{ind} ~14).

Table 3. Gold(I) local structure in Au_2S and $Na_3Au(S_2O_3)_3 \cdot 2H_2O$ crystalline solids and Au thiosulfate aqueous complex at ambient conditions, derived from fitting EXAFS spectra at Au L_3-edge [a], and their comparison with X-ray diffraction (XRD) data.

compound	atom	N (atoms)	R (Å)	σ^2 (Å^2)	Δe (eV)	P-factor	XRD data
$Na_3Au(S_2O_3)_2 \cdot 2H_2O$ (s) [b]	S1	2.2±0.2	2.295±0.005	0.003	8.5	0.020	2 S at 2.27-2.28 Å
	S2	2.0±1.0	3.41±0.03	0.01			1 Au at 3.30 Å
	Au	ND [e]	ND	ND			2 S at 3.41-3.42 Å
	O	ND	ND	ND			7 O at 3.52-3.86 Å
	ms1 [d]	2.0	4.60	0.005			
	ms2 [d]	2.0	4.60	0.005			
0.002 m $Na_3Au(S_2O_3)_2$ aqueous solution, *pH*~7	S1	1.9±0.2	2.310±0.006	0.002	7.5	0.007	
	S2	ND	ND	ND			
	O	ND	ND	ND			
	ms1 [d]	2.0	4.62	0.01			
	ms2 [d]	2.0	4.62	0.01			
Au_2S (s) [c]	S1	2.0±0.2	2.30±0.01	0.003	7.5	0.011	2S at 2.17 Å
	Au	ND	ND	ND			12 Au at 3.55 Å
	S2	ND	ND	ND			6 S at 4.16 Å
	ms1 [d]	2.0	4.60	0.006			
	ms2 [d]	2.0	4.60	0.006			
EXAFS fit error				±30%	±1.0		

[a] see Table 2 for explanation of EXAFS parameters

[b] purchased from Alfa Aesar; XRD data from Ruben et al. (1974)

[c] Synthetic crystalline phase characterized in details in Gurevich et al. (2004); XRD data from Ishikawa et al. (1995); the difference of > 0.1 Å between Au-S1 distances from EXAFS and XRD data, and the absence of EXAFS signal from the next-nearest heavy atoms (Au and S) might indicate partial amorphization of Au_2S during storage and/or X-ray beam exposure.

[d] Multiple scattering paths within the linear S1-Au-S1' unit: Au-S1-S1'-Au and Au-S1-Au-S1'-Au with R and N values defined as: $R_{ms1,2} = 2 \times R_{Au-S1}$, $N_{ms1,2} = N_{S1}$.

[e] ND = not detected by EXAFS

Table 4. Steady-state gold and sulfur aqueous concentrations in aqueous solutions S-NaOH-Na_2SO_4-H_2SO_4 saturated with metallic gold, derived from the X-ray absorption spectra at Au L_3-edge as a function of temperature at 600 bar (except indicated).

# Run initial composition [a]	T(°C)	fluid density [c] (g/cm^3)	Sulfur [d] (mol/kg fluid)	$\Delta\mu$ [e]	C_{Au} [f] (mol/kg fluid)	$\log_{10}(m_{Au})$ [g]
# 1	300	0.95	4.0±0.5	0.97	0.123	-0.82±0.05
3.48mS-2.17m NaOH						
	300	0.91	2.3±0.2	0.417	0.055	-1.20±0.05
# 2	350	0.85	2.3±0.2	0.396	0.056	-1.19±0.10
2.66m S-1.42m NaOH	400	0.70	1.5±0.5	0.204	0.035	-1.39±0.10
	450	0.60	1.0±0.5	0.059	0.012	-1.87±0.15
# 3	300	0.82	0.50±0.03	0.066	0.010	-2.00±0.05
0.53m S-0.40m NaOH	400	0.66	0.50±0.05	0.038	0.0068	-2.15±0.10
	450	0.53	0.50±0.05	0.014	0.0033	-2.46±0.15
# 4 [b]	200	0.91	0.55±0.05	0.028	0.0036	-2.42±0.10
0.58m S-0.40m NaOH	300	0.79	0.50±0.05	0.082	0.0124	-1.89±0.10
	400	0.47	0.4±0.1	0.0082	0.0021	-2.66±0.30
# 5	300	0.80	0.5±0.3	0.0055	8×10^{-4}	-3.1±0.3
1.0m S-H_2O	400	0.65	0.75±0.20	0.0029	5×10^{-4}	-3.3±0.3
# 6	400	0.65	ND [h]	$< 10^{-3}$	$< 2\times10^{-4}$	< -3.7
0.50m S-H_2O	450	0.55	ND	$\leq 10^{-3}$	$\leq 2\times10^{-4}$	≤ -3.7
# 7	300	0.80	≤ 0.2	1.2×10^{-3}	$\sim 2\times10^{-4}$	-3.7±0.5
0.64m S-H_2O	400	0.65	0.7±0.3	$\leq 5\times10^{-4}$	$\leq 1\times10^{-4}$	≤ -4.0
# 8	400	0.65	0.6±0.1	$\leq 5\times10^{-4}$	$\leq 1\times10^{-4}$	≤ -4.0
0.81m S-H_2O	450	0.55	0.6±0.3	$\sim 9\times10^{-4}$	$\sim 2\times10^{-4}$	-3.7±0.5
#9	300	0.87	ND	0.0084	0.0011	-2.9±0.2
0.51m S-0.55m Na_2SO_4	400	0.72	ND	0.0013	2.1×10^{-4}	-3.6±0.3
#10	400	0.73	ND	0.0035	5.7×10^{-4}	-3.2±0.2
0.79m S-0.55m Na_2SO_4						
# 11	400	0.68	ND	0.0010	$\leq 2\times10^{-4}$	-3.7±0.5
1.0m-0.92m H_2SO_4						

[a] Initial compositions are expressed in molality (number of moles per kg of water).

[b] At 300 bar.

[c] Fluid density is calculated assuming that it is similar to that of a NaCl-H_2O solution of the same concentration (wt%) as the experimental Na-S-H_2O-Au fluid, and using the PVTX properties of NaCl aqueous solutions calculated using the Fluids software (Bakker, 2003).

[d] Dissolved sulfur concentration is estimated from the absorbance before the Au-edge (11.7 keV) of transmission spectra, they are expressed in mol/kg of fluid.

[e] Height of the absorption amplitude over Au L_3-edge as derived from transmission spectra.

[f] Au total dissolved concentration (in mol/kg of fluid) calculated using Eqn. (1) in Electronic annex EA-1, and setting the X-ray beam path inside the cell at 0.38±0.02 cm based on Eqn (1) and using the measured absorption-edge height for a 0.035m $HAuCl_4$-0.504m NaCl-0.01m HCl solution at 30°C/600 bar, and a change of gold total absorption cross-section over Au L_3-edge, $\Delta\sigma_{Au}$, of 111.14 $cm^2\ g^{-1}$ (Elam et al., 2002).

[g] Decimal logarithm of Au molality (mol/kg H_2O) derived from measured Au concentration and solution composition. Uncertainties on the values stem from those associated with the determination of the absorption edge height, X-ray path length, and solution density (see EA-1).

[h] ND = not determined

975 **Table 5**. Equilibrium constants for reactions controlling gold solubility derived in this study [a].

Reaction	T (°C)	P (bar)	$\log_{10}K$
$Au_{(s)} + 2\ H_2S^0_{(aq)} = Au(HS)H_2S^0_{(aq)} + 0.5\ H_{2(g)}$	300	600	-2.6±0.5
	400	600	-4.0±0.5
	450	600	-4.2±0.7
$Au_{(s)} + H_2S^0_{(aq)} + SO_2{}^0_{(aq)} = Au(HS)SO_2{}^0_{(aq)} + 0.5\ H_{2(g)}$	300	600	-1.5±0.7
	400	600	-3.7±0.5
	450	600	-3.9±0.7
$Au_{(s)} + H_2S^0_{(aq)} + HS^- = Au(HS)_2^- + 0.5\ H_{2(g)}$	200	300	-2.4±0.2
	300	300	-1.3±0.2
	400	300	-1.4±0.4
	300	600	-1.4±0.1
	350	600	-1.2±0.2
	400	600	-1.1±0.3
	450	600	-1.3±0.7

[a] Equilibrium constants were generated using Au concentrations from Table 4 as measured by XAFS and assuming the dominant presence of either $Au(HS)H_2S^0$(aq) or $Au(HS)SO_2{}^0$(aq) as the two most probable candidates at acidic
980 conditions (*pH* < ~3, exp # 5-8 and 11) and of $Au(HS)_2^-$ in near-neutral solutions (*pH* 6-8, exp # 1-4). See Table A1 for concentrations of other reaction constituents. Activity coefficients of neutral species were approximated to unity, whereas those of charged species were calculated using the extended Debye-Hückel equation (A1).

Figure Captions

Fig. 1. (A) Distribution of Au-sulfide species in a 0.5m S-NaOH aqueous solution according to the 'classical' Au speciation scheme at 300 (dashed curves) and 400°C (solid curves) at 600 bar, and (B) solubility of metallic gold in aqueous solution as a function of *pH* in the system Au(s) – H_2O – 0.5m S – NaOH at 400°C and 600 bar for typical conditions of the XAFS experiments. The thermodynamic properties of Au complexes are taken from the compilation of Akinfiev et al. (2008); those for S species and other solution constituents from SUPCRT 2007 (Johnson et al., 1992; *http://geopig.asu.edu/index.html#*). The solubility maximum at *pH* ~7 roughly corresponds to the H_2S-HS^- equal-activity point, according to the dominant solubility reaction Au(s) + H_2S^0(aq) + HS^- = $Au(HS)_2^-$ + 0.5 H_2(g). See text and Appendix for further details and comparison with other data sources.

Fig. 2. Distribution of major sulfur forms in aqueous solution in the systems H_2O–0.5m S, H_2O–0.5m S–0.5m Na_2SO_4, and H_2O–0.5m S–0.4m NaOH at 400°C and pressures 400-1000 bar for conditions typical of XAFS experiments, according to thermodynamic data from SUPCRT 2007 database (Johnson et al., 1992; *http://geopig.asu.edu/index.html#*) and available experimental data indicated in the figure. Numerous minor S species (< 0.1% of total S) are not shown for clarity. See text and Table A1 for more details.

Fig. 3. Optimized geometries of selected aurous sulfide and sulfite species in aqueous solution calculated using MP2 quantum-chemical methods (see Table 1 for details).

Fig. 4. Normalized XANES spectra of selected Au-S solutions at 600 bar and indicated temperatures (in °C) obtained in this study, and reference solids and aqueous species, and schematic structure of the Au-thiosulfate moiety. The spectrum of the aurous gold thiosulfate aqueous complex was recorded in this study from 0.002m $Na_3Au(S_2O_3)_2$ solution at *pH* ~7 and ambient *T-P*; the spectrum of the aurous gold chloride aqueous complex ($AuCl_2^-$) was taken from Pokrovski et al. (2009). The vertical dashed lines denote two main resonances at ~11923 eV (feature A) and ~11929-11932 eV (feature B) apparent in the spectra of all Au-S aqueous species. Note that the relative amplitude of feature A grows systematically from neutral to acid *pH* in H_2O-S-Na_2SO_4-NaOH solutions and attains a maximum in the $Au(S_2O_3)_2^{3-}$ species; whereas the amplitude of feature B slighly decreases from neutral to acidic solutions and further weakens in the Au-thiosulfate aqueous solution and solid, and exhibits an energy shift of the its maximum by ~2 eV (shown by a third shorter dashed vertical line). This might indicate the presence of Au-S-S (and probably Au-S-O) bonds in acidic S-rich solutions of this study, similarly to Au thiosulfate solid and solution. The damping of the amplitude of both features in the thiosulfate solid might be due to larger structural disorder of the Au sites in the solid in comparison to the smaller and more symmetrical Au-thiosulfate species in aqueous solution.

Fig. 5. Normalized k^2-weighted EXAFS spectra from selected experiments in aqueous Au-S-Na_2SO_4-NaOH solutions at 600 bars and indicated temperatures (in °C), and their corresponding Fourier Transform (FT) magnitudes (not corrected for phase shift). Vertical dashed lines on the FT spectra denote the signals from the nearest S1 atomic shell, multiple scattering (MS) within the linear S-Au-S cluster, and a possible next-nearest S2 contribution. The spectrum of the $Au(S_2O_3)_2^{3-}$ complex was recorded at ambient *T-P* from 0.002m $Na_3Au(S_2O_3)_2$ solution of *pH* ~7. Feature S2 might correspond to the 2nd shell sulfur in the Au-S_2O_3 unit, but could not be detected unambiguously in aqueous solution (see text and Table 3 for details).

Fig. 6. Evolution of gold molality in solution, determined from the absorption edge height of the spectrum using equation (1) in EA-1, as a function of time and temperature at 600 bars in two representative experiments at near-neutral *pH* containing an excess of metallic gold and with fluid compositions indicated in the figure (exp #2 (A) and #3 (B), see Table 4). Each symbol corresponds to a XAFS scan; arrows indicate temperature changes during the experiment; dashed horizontal lines (where present) denote the steady-state Au concentration at each temperature. Large grey error bars stand for the range of Au dissolved concentrations in equilibrium with metallic gold at each temperature as calculated using the stability constants for the $Au(HS)_2^-$ complex from available literature sources (see Table A2).

Fig. 7. Evolution of gold molality in solution, determined from the absorption edge height of the spectrum (equation (1) in EA-1) as a function of time and temperature at 600 bars at acidic *pH* (*pH* $\leq$ 5) in experiments with an excess of metallic gold, carried out in the systems H_2O-S (A) and H_2O-S-Na_2SO_4 (B) at indicated compositions. Each symbol corresponds to a XAFS scan; arrows indicate temperature changes during the experiment; dashed horizontal lines (where present) denote the steady-state Au concentrations at each temperature. The grayed band in panel (A) stands for the range of Au concentrations measured in experiments # 6, 7 and 8 (see Table 4); symbols were omitted for clarity. Error bars denote the range of Au aqueous concentrations in equilibrium with metallic gold at each temperature as calculated using the stability constants for the $AuHS^0$ and $Au(HS)_2^-$ complexes from available literature sources (see text and Table A2).

Printed Appendix

Details of equilibrium calculations of gold and sulfur speciation and solubility in the experiments of this study and their comparison with available literature data

Gold and sulfur chemical speciation and solubility in aqueous solution were simulated via equilibrium thermodynamic calculations and compared with experimental data. Modeling was performed using the HCh software package (Shvarov, 1999) based on the minimization of the Gibbs free energy of the system.

The thermodynamic properties of the major fluid constituents like H_2O, H^+, OH^-, Na^+, $NaOH^0$(aq) H_2^0(aq) and most aqueous sulfur species (sulfides, sulfites, sulfates, thiosulfates, and polysulfides) were taken from the SUPCRT 2007 database based on the revised HKF equation of state (Johnson et al., 1992; Shock et al., 1989, 1992, 1997; Sverjensky et al., 1997; Schulte et al., 2001; http://geopig.asu.edu/index.html#). Although an alternative thermodynamic model has recently been proposed for some volatile sulfur species (H_2S^0(aq), SO_2^0(aq), Akinfiev and Diamond, 2003), the SUPCRT data were adopted (Schulte et al., 2001) to maintain the internal consistency with the corresponding sulfide and sulfite anions whose thermodynamic properties rely on those for H_2S^0(aq) and SO_2^0(aq). Differences in the Gibbs free energies of H_2S^0(aq) and SO_2^0(aq) between the two models do not exceed 2 and 5 kJ/mol, respectively, and thus yield only minor effect on the calculated Au speciation and solubility at *T-P* conditions of this study. The stability constant of $NaHS^0$(aq) ion pair was assumed to be equal to that of $NaCl^0$(aq) adopted from Ho et al. (1994); that of $NaSO_4^-$ was taken from Pokrovski et al. (1995). Thermodynamic properties of solid and liquid sulfur were taken from the JANAF database (Chase et al., 1998); those for Au(s), H_2(g) and H_2S(g) were adopted from Robie and Hemingway (1995). Activity coefficients (γ_i) of charged species were calculated using the extended Debye-Hückel equation:

$$\log \gamma_i = -A\, z_i^2 \sqrt{I}/(1+B\, å_i \sqrt{I}) + \Gamma_\gamma + b_{NaCl}\, I\,, \qquad \text{(A1)}$$

where A and B refer to the Debye-Hückel electrostatic parameters and were taken from Helgeson and Kirkham (1974); I is the effective molal ionic strength ($I = 0.5 \sum(z_i^2 m_i)$); z_i and $å_i$ represent the ion charge and the distance of the closest approach for i*th* species, respectively; Γ_γ designates the mole fraction to molality conversion factor, $\Gamma_\gamma = \log(1+0.018m^*)$, where m* stands for the sum of the molalities of all solute species; and b_{NaCl} is the extended term parameter for NaCl-dominated solutions, which is a function of temperature and pressure (Oelkers and Helgeson, 1990). The values of $å_i$ are calculated according to Shock et al. (1992). For activity coefficients of neutral species, equation (A1) reduces to $\log \gamma_i = \Gamma_\gamma + b_i I$, where b_i is the empirical Setchenov coefficient for each neutral complex. Because of the extreme scarcity of Setchenov coefficients for the majority of neutral species in high-temperature solutions, a zero value for b_i was adopted in the present study which yields activity coefficients for all neutral species close to one.

The calculated concentrations of the major S species in each XAFS experiment are reported in Table A1. The uncertainties of the calculated values of *pH* and species amounts are a direct function of the uncertainties associated with the chosen thermodynamic data for the main solution components (particularly $H_2S^0/HS^-/NaHS^0$, $HSO_4^-/SO_4^{2-}/NaSO_4^-$). At $T \leq 350$°C, these uncertainties yield typical errors in *pH* of 0.2-0.4 unit. At supercritical temperatures ($T \geq 400$°C), errors of calculated *pH* may attain 0.5-1.0 unit. The concentrations of the main sulfur species are affected accordingly.

The last column of Table A1 lists the molal ratio $Au(HS)_2^-/Au(HS)^0$ in the experimental solutions calculated using thermodynamic properties of these complexes from Akinfiev et al. (2008). This is the most recent compilation of thermodynamic properties for aqueous Au species, which complements the thermodynamic database of Akinfiev and Zotov (2001). The compilation is based on the HKF (Helgeson-Kirkham-Flowers) model. Thermodynamic properties and HKF equation-of-state parameters for $Au(HS)_2^-$ were generated by the authors via the regression of experimental data from Berndt et al. (1994), Shenberger and Barnes (1989), Stefánsson and Seward (2004), and Tagirov et al. (2005, 2006). For $Au(HS)^0$, the following solubility data were used, assuming in all cases a stoichiometry AuHS for complexes in acidic solution: Hayashi and Ohmoto (1991), Gibert et al. (1998), Baranova and Zotov (1998), Stefánsson and Seward (2004), and Tagirov et al. (2005, 2006). Note that Akinfiev et al. (2008)

used the original experimental gold solubility data from these studies, rather than stability constants reported by the different authors. The Gibbs free energies of Au complexes at a given *P* and *T* were calculated from the original data points, in accordance with the chosen speciation model; they were subsequently regressed to derive the standard thermodynamic properties and HKF equation-of-state parameters for $AuHS^0$ and $Au(HS)_2^-$. To evaluate the role of Au-hydroxide complexes, we used the HKF equation-of-state parameters calculated by Akinfiev and Zotov (2001) from experimental data of Zotov et al. (1995). The concentrations of $AuOH^0$ and $Au(OH)_2^-$ do not exceed 1% of the total dissolved Au in all our experiments.

Table A2 compares XAFS-derived solubilities with those calculated using stability constants for Au-sulfide complexes reported in the literature from solubility studies. Only experimental studies attempting to derive the stoichiometry of As-S complexes were considered in the Table. Note that only original experimental values of constants, as they are reported in these studies, were used. In the absence of systematic *P*-dependent measurements in most studies, the effect of pressure on the stability constants was assumed to be negligible. In addition to experimental works, were also included two major theoretical studies (Sverjensky et al., 1997; Akinfiev et al., 2008) that employed a regression of selected available Au solubility data in the framework of the revised HKF model (see footnote of Table A2 for details and text for discussion).

Table A1. Sulfur species concentrations (expressed as decimal logarithm of molality), hydrogen fugacity, *pH*, and $Au(HS)_2^-/AuHS^0$ concentration ratio in the experimental solutions of this study, predicted using available thermodynamic data.

T,°C	S_{total}	$H_2S^0_{(aq)}$	HS^-	$NaHS^0_{(aq)}$	HSO_4^-	SO_4^{2-}	$NaSO_4^-$	$SO_2^0{}_{(aq)}$	HSO_3^-	SO_3^{2-}	$S_2O_3^{2-}$	$HS_2O_3^-$	$H_2S_2O_3$
#1, 600 bar, 3.48m S-2.17m NaOH													
300	0.53	0.26	-0.64	-0.92	-2.21	-0.80	-0.19	-5.37	-4.38	-7.13	-2.39	-5.23	-8.78
#2, 600 bar, 2.66m S-1.42m NaOH													
300	0.38	0.16	-0.90	-1.30	-2.05	-0.89	-0.35	-4.93	-4.32	-7.36	-2.63	-5.14	-8.47
350	0.42	0.28	-1.21	-1.35	-1.63	-0.96	-0.33	-3.69	-3.72	-7.21	-2.71	-4.85	-7.86
400	0.42	0.28	-1.20	-1.30	-1.51	-0.84	-0.30	-3.27	-3.42	-6.72	-2.60	-5.05	-7.99
450*	0.42	0.28	-1.15	-1.45	-1.83	-0.33	-0.71	-3.04	-3.32	-5.77	-2.45	-5.52	-8.34
#3, 600 bar, 0.53m S-0.40m NaOH													
300	-0.28	-0.60	-0.97	-1.68	-3.22	-1.49	-1.00	-6.70	-5.13	-7.67	-3.95	-7.11	-11.24
400	-0.28	-0.60	-1.10	-1.29	-3.05	-1.73	-0.95	-5.39	-4.47	-7.62	-6.37	-7.28	-11.05
450*	-0.28	-0.59	-1.26	-1.13	-3.20	-1.56	-1.98	-4.95	-4.38	-7.10	-4.46	-7.77	-11.15
#4, 300 bar, 0.58m S-0.40m NaOH													
200	-0.24	-0.52	-1.04	-2.15	-3.44	-1.19	-1.11	< -8	-6.26	< -8	-3.53	-6.92	-11.05
300	-0.24	-0.50	-1.07	-1.74	-3.05	-1.52	-0.95	-6.28	-5.08	-7.84	-3.97	-6.91	-10.84
400*	-0.24	-0.48	-1.17	-1.45	-4.58	-0.85	-2.43	-5.47	-5.67	-5.66	-4.07	-9.07	-11.97
#9, 600 bar, 0.51m S-0.55m Na_2SO_4													
300	-0.08	-0.67	-3.00	-3.46	-0.81	-0.98	-0.42	-3.26	-3.92	-8.30	-3.57	-4.74	-6.79
400	0.03	-0.42	-2.97	-3.07	-0.61	-1.06	-0.46	-1.98	-3.11	-8.01	-3.52	-4.67	-6.39
#10, 600 bar, 0.79m S-0.55m Na_2SO_4													
300	-0.08	-0.67	-3.00	-3.46	-0.81	-0.98	-0.42	-3.26	-3.92	-8.30	-3.57	-4.74	-6.79
400	0.13	-0.23	-3.08	-0.51	-0.48	-1.10	-0.52	-1.31	-3.04	-7.74	-3.50	-4.43	-6.02
#5-8, 600 bar, 0.5-1.0 m S-H_2O													
300	-1.12	-1.26	-6.30	NA	-1.81	-5.28	NA	-2.37	-5.48	< -13	-8.42	-6.30	-5.63
400	-0.32	-0.49	-6.22	NA	-2.21	-6.82	NA	-0.81	-5.12	< -13	-9.35	-6.33	-4.87
450	-0.10	-0.30	-6.44	NA	-2.94	-8.00	NA	-0.57	-5.76	< -13	< -10	-7.21	-5.11
#11, 600 bar, 1.0m S-0.92 H_2SO_4													
400	0.18	-0.68	-6.87	NA	-1.71	-6.52	NA	0.16	-4.91	< -13	-9.36	-6.11	-4.35

Table A1 - continued

T,°C	S_2^{2-}	S_3^{2-}	S_4^{2-}	S_5^{2-}	log *f* H_2, bar	H_2^0(aq)	pH	$\frac{m(Au(HS)_2^-)}{m(AuHS)}$
#1, 600 bar, 3.48m S-2.17m NaOH								
300	-3.82	-2.43	-2.00	-1.64	-1.95	-4.52	5.7	$2.9 \cdot 10^3$
#2, 600 bar, 2.66m S-1.42m NaOH								
300	-4.34	-3.10	-2.66	-2.34	-2.05	-4.62	5.6	$1.6 \cdot 10^3$
350	-3.93	-3.55	-3.28	-3.12	-1.80	-4.12	5.7	$6.0 \cdot 10^2$
400	-4.61	-3.47	-3.49	-3.62	-1.47	-3.50	6.0	$4.7 \cdot 10^2$
450	-3.95	-3.27	-3.82	-4.40	-1.12	-2.74	6.5	$5.1 \cdot 10^2$
#3, 600 bar, 0.53m S-0.40m NaOH								
300	-4.96	-4.55	-5.12	-5.77	-1.78	-4.38	6.4	$1.4 \cdot 10^3$
400	-5.16	-5.30	-6.60	-7.96	-1.04	-3.09	7.2	$6.4 \cdot 10^2$
450	-5.03	-5.74	-7.58	-9.49	-0.76	-2.40	7.9	$4.2 \cdot 10^2$
#4, 300 bar, 0.58m S-0.40m NaOH								
200	-4.35	-3.82	-3.58	-3.41	-2.99	-5.91	5.8	$2.8 \cdot 10^3$
300	-4.33	-4.72	-5.23	-5.53	-1.90	-4.39	6.4	$1.3 \cdot 10^3$
400	-2.67	-4.67	< -6	< -8	-0.82	-2.20	8.1	$4.5 \cdot 10^2$
#9, 600 bar, 0.51m S-0.55m Na_2SO_4								
300	< -6	< -6	< -6	< -6	-2.92	-5.45	4.4	13
400	< -6	< -6	< -6	< -6	-2.16	-4.17	4.9	8
#10, 600 bar, 0.79m S-0.55m Na_2SO_4								
300	< -7	< -6	< -6	-5.80	-2.88	-5.45	4.4	13
400	< -6	< -6	< -6	< -6	-2.20	-4.23	4.7	7
#5-8, 600 bar, ~0.7m S-H_2O								
300	< -10	< -10	< -10	< -10	-3.47	-6.04	1.9	$6.0 \cdot 10^{-3}$
400	< -10	< -10	< -10	< -10	-2.55	-4.58	2.3	$8.3 \cdot 10^{-3}$
450	< -10	< -10	< -10	< -10	-2.14	-3.76	3.0	$7.1 \cdot 10^{-3}$
#11, 600 bar, 1.0m S-0.92 H_2SO_4								
400	< -13	< -13	< -13	< -13	-3.02	-5.05	1.6	$4.6 \cdot 10^{-4}$

See Appendix text for data sources for S and Au species. NA = not available, the corresponding compound is absent in the experiment. Concentrations of polythionate species ($S_2O_{4,5,6,8}$ and $S_{3,4,5}O_6$) are below 10^{-10} m in all solutions. * = calculated concentrations of SO_4^{2-} (and, consequently, related species HSO_4^-, $NaSO_4^-$) may be unreliable at indicated conditions mostly due to underestimation of activity coefficients for highly charged ions at low fluid densities (<0.35 g/cm^3, an 'official' limit for the HKF model). Nevertheless, this does not affect significantly the concentrations of other major sulfide species and H_2 fugacity.

Table A2. Comparison between gold solubility (expressed as decimal logarithm of Au molality in solution) in the system $Au_{(s)}$-H_2O-S-NaOH-Na_2SO_4 measured in this study and calculated according to available experimental and theoretical studies from the literature. [a]

T°C	This study [b]	Tag 2005, 2006 [c]	Ste/Sew 2004 [d]	Fle/Kni 2000 [e]	Dad 2000 [f]	Lou/Mav 1999 [g]	Gib 1998 [h]	Pan/Woo 1994 [i]	Hay/Ohm 1991 [j]	She/Bar 1989 [k]	Sve 1997 [l]	Aki 2008 [m]
# 1, 600 bar: 3.48m S-2.17m NaOH												
300	-0.82±0.05	NA	-0.8±0.1	-1.2±0.4	-0.9±0.3	-0.3	NA	-1.5±0.6	NA	-0.8±0.3	-0.8	-0.9±0.3
# 2, 600 bar: 2.66m S-1.42m NaOH												
300	-1.20±0.05	NA	-1.1±0.1	-1.3±0.4	-1.3±0.3	-0.4	NA	-1.8±0.5	NA	-1.3±0.2	-1.2	-1.2±0.3
350	-1.19±0.10	-1.5±0.4	-1.5±0.1	-1.4±0.4	NA	-0.4	NA	-2.0±0.4	NA	-1.3±0.3	-1.3	-1.6±0.3
400	-1.39±0.10	-2.0±0.5	-1.8±0.1	-1.2±0.4	NA	-0.5	NA	NA	NA	NA	-1.3	-1.9±0.5
450	-1.87±0.15	-2.0±0.4	-1.8±0.2	-1.1±0.6	NA	-1.2	NA	NA	NA	NA	-1.2	-2.1±0.7
# 3, 600 bar: 0.53m S-0.40m NaOH												
300	-2.00±0.05	NA	-2.0±0.1	-2.5±0.4	-2.2±0.3	-1.4	NA	-2.8±0.5	NA	-2.2±0.2	-2.0	-2.2±0.3
400	-2.15±0.10	-2.9±0.4	-2.7±0.1	-2.3±0.3	NA	-2.3	NA	NA	NA	NA	-2.1	-2.8±0.5
450	-2.46±0.15	-3.4±0.4	-3.1±0.2	-2.3±0.6	NA	-3.9	NA	NA	NA	NA	-2.2	-3.3±0.5
# 4, 300 bar: 0.58m S-0.40m NaOH												
200	-2.42±0.10	-1.8±0.4	-1.5±0.1	-2.7±0.4	NA	-1.1	NA	-2.2±0.5	NA	-1.6±0.2	-2.0	-1.7±0.2
300	-1.89±0.10	NA	-2.0±0.1	-2.4±0.4	-2.3±0.3	-1.3	NA	-2.7±0.5	NA	-2.0±0.2	-1.9	-2.1±0.3
400	-2.66±0.30	-2.8±0.5	-2.8±0.1	-2.4±0.3	NA	-3.8	NA	NA	NA	NA	-2.2	-3.3±0.5
# 5, 6, 7, 8, 600 bar: 0.5-1.0m S-H_2O												
300	$\leq$ -3.7	NA	-5.1±0.1	NA	-3.2±0.2	-1.7	NA	NA	-4.5±0.3	NA	NA	-5.1±0.5
400	-3.7±0.4	-5.4±0.5	-4.9±0.1	NA	NA	-1.3	-4.5±0.3	NA	-3.5±0.5	NA	NA	-4.7±0.5
450	-3.7±0.5	NA	-5.4±0.2	NA	NA	-2.2	-4.6±0.4	NA	-4.0±0.5	NA	NA	-5.1±0.5
# 9, 600 bar: 0.51m S-0.55m Na_2SO_4												
300	-2.9±0.2	NA	-3.6±0.1	-4.0±0.4	-2.9±0.3	-1.1	NA	-4.4±0.5	-3.6±0.3	-3.6±0.2	-3.6	-3.7±0.3
400	-3.6±0.3	-4.1±0.5	-3.9±0.1	-3.0±0.3	NA	-1.5	-4.6±0.3	NA	-3.9±0.5	NA	-3.2	-4.0±0.3
# 10, 600 bar: 0.79m S-0.55m Na_2SO_4												
400	-3.2±0.2	-4.0±0.5	-3.7±0.1	-2.8±0.3	NA	-1.2	-4.4±0.3	NA	-3.5±0.5	NA	-3.1	-3.8±0.3
# 11, 600 bar: 1.0m S-0.92m H_2SO_4												
400	-3.7±0.5	-5.5±0.5	-5.1±0.1	NA	NA	-2.6	-4.7±0.3	NA	-4.0±0.5	NA	NA	-4.9±0.5

[a] For consistency, thermodynamic properties of the major fluid constituents and S-bearing species were taken from the SUPCRT database (Johnson et al., 1992; http://geopig.asu.edu/index.html#). Uncertainties on calculated Au solubilities stem from 1) those reported in the corresponding experimental or theoretical studies on Au complex stabilities; 2) differences in thermodynamic data sources for the main S species used by different authors. See Appendix text for disscussion of additional uncertainties related to the sulfur speciation.

[b] see Table 4 for details.

[c] Tagirov et al. (2005) measured the solubility of gold at 350-500°C and 0.5 and 1 kbar in the presence of sulfide and silicate mineral assemblages buffering *pH*, $f(H_2)$ and $f(S_2)$, and determined the formation constants for $Au(HS)^0$ and $Au(HS)_2^-$. Stability constants determined at 1 kbar were adopted in our calculations at all pressures. Tagirov et al. (2006) measured the solubility of Au-Ag-S phases at 25°C and $AgAuS_{(s)}$ to 250°C and P_{sat}, and determined the stability of $Au(HS)^0$ at 25°C and $Au(HS)_2^-$ from 25 to 250 °C.

[d] Stefánsson and Seward (2004) measured the solubility of metallic gold in sulfide solutions at 100-500°C and 500 bars, using a flow-through reactor with control of dissolved H_2S and hydrogen concentration, and reported the stability constants for $AuHS^0$ and $Au(HS)_2^-$. Because their data yield very similar results as those of previous studies of the same group (Seward, 1973; Benning and Seward, 1996), these latter studies were not included in Table A2.

[e] Fleet and Knipe (2000) measured gold solubility in the MgS-H_2O system with H_2S concentrations up to 20.6 m, from 100 to 400°C at 1.5 kbar and pH_T = 4.3-5.8. Their original stability constants for $Au(HS)_2^-$ (their eqn(1),) were regressed versus 1/T(K), and the newly generated equation ($\log K_{Au(HS)_2^-} = -2642.5/T(K) + 2.85$; correlation coefficient R^2= 0.9997) was used for the temperature range 200-450°C. The effect of pressure was assumed to be insignificant.

[f] Dadze et al. (2000) reported stability constants for AuHS and $Au(HS)_2^-$ obtained from gold solubility measurements in thioacetamide solutions at 300°C and 300 bars. The same constant values were used at 600 bar. No temperature extrapolation is possible.

[g] Loucks and Mavrogenes (1999) reported HKF parameters for $AuHS(H_2S)_3^0$, generated from gold solubility measurements at 500-650°C and 1-4 kbar. Errors associated with these parameters were not reported.

[h] Gibert et al. (1998) reported stability constants for $AuHS^0$ at 350-450 °C and 500 bar, obtained from Au solubility measurements in the presence of pyrite-pyrrhotite-magnetite, pyrite-magnetite-hematite and quartz-muscovite-potassium feldspar assemblages.

[i] Pan and Wood (1994) reported stability constants for $Au(HS)_2^-$ at 200-350°C and P_{sat} from gold solubility measurements in NaHS-Na_2SO_4 solutions with ΣS = 0.3-2.2 m.

[j] Hayashi and Ohmoto (1991), using log K= -5.1±0.3 for the reaction $Au(s) + 2\ H_2S^0(aq) = HAu(HS)_2^0(aq) + 0.5\ H_2^0(aq)$ reported in the original work of gold solubility between 250 and 350°C at P_{sat} and pH_T = 1.9-5.0. This constant value was adopted in our calculations at 300 to 450°C and 600 bar.

[k] Shenberger and Barnes (1989) reported formation constants of $Au(HS)_2^-$ derived from gold solubility measurements in H_2-sulfide-sulfate-phosphate solutions from 150 to 350°C and P_{sat}.

[l] Sverjensky et al. (1997) retrieved $Au(HS)_2^-$ HKF parameters from the experimental data of Shenberger and Barnes (1989) and using the HKF equation of state; no uncertainties were reported.

[m] Akinfiev et al. (2008) compiled the available literature data and calculated the standard thermodynamic properties and HKF equation-of-state parameters for $Au(HS)^0$ and $Au(HS)_2^-$.

NA = not available or could not be extrapolated.

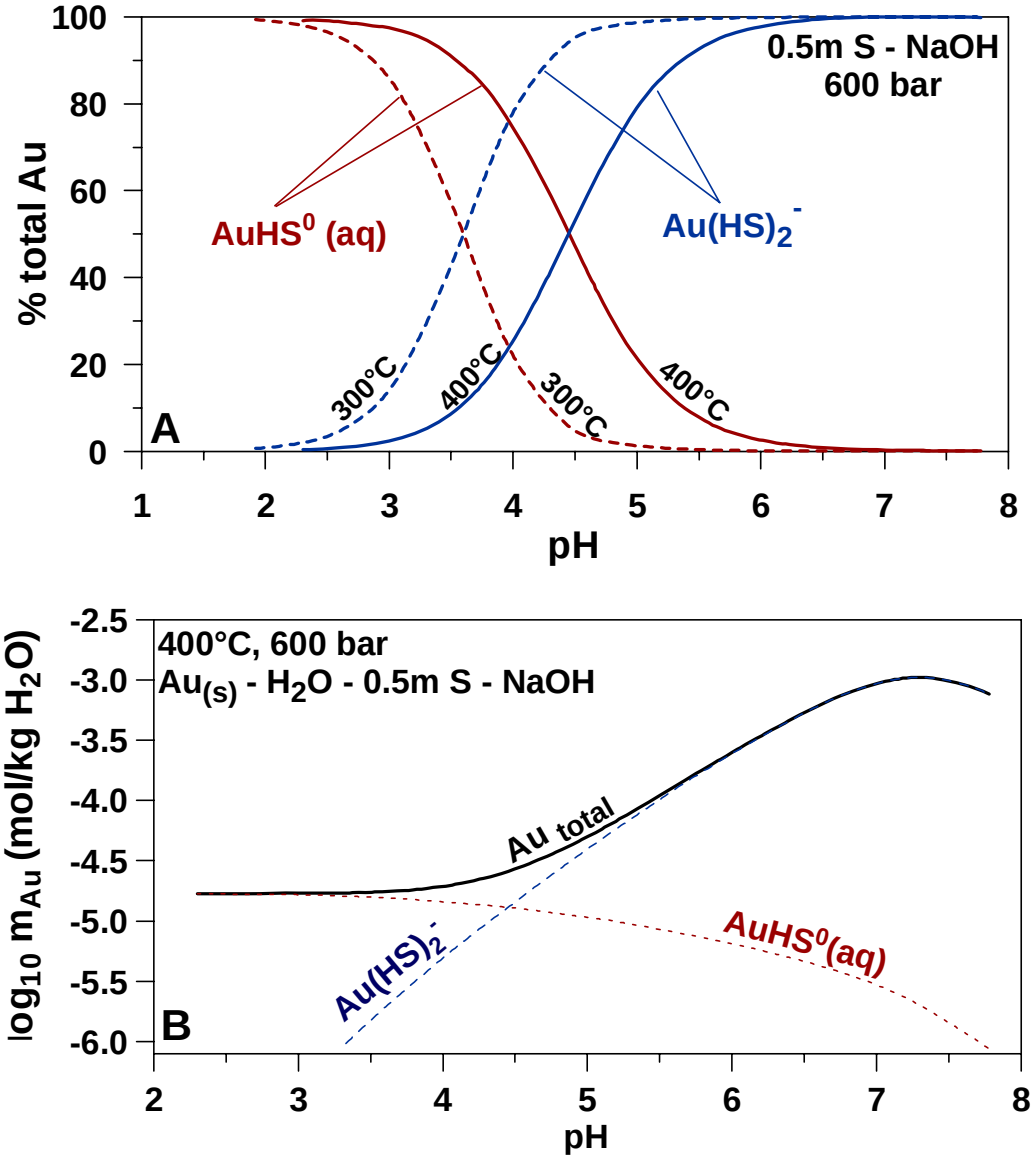

W6365_revised-Fig. 1

400°C, 400-1000 bar, 0.5m S - H_2O, pH ~ 2-3

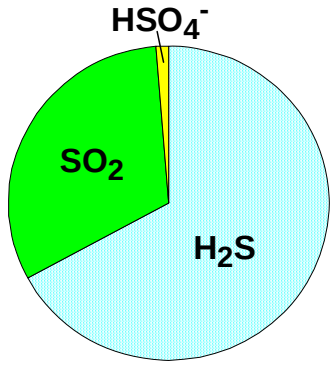

Thermodynamic predictions
(SUPCRT 07)

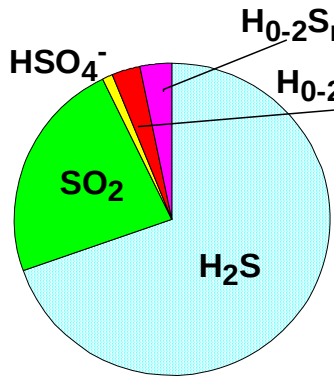

Batch-reactor
(Sorokin and Dadze, 1994)

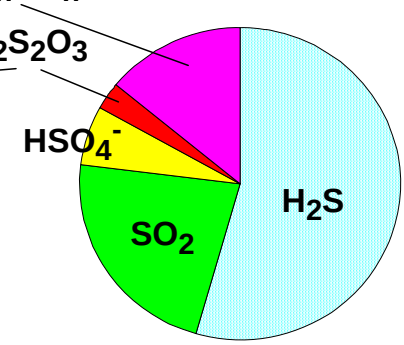

In situ Raman spectroscopy
(Bondarenko and Gorbaty, 1997)

400°C, 600 bar,
0.5m S - 0.5m Na_2SO_4 - H_2O, pH ~ 5

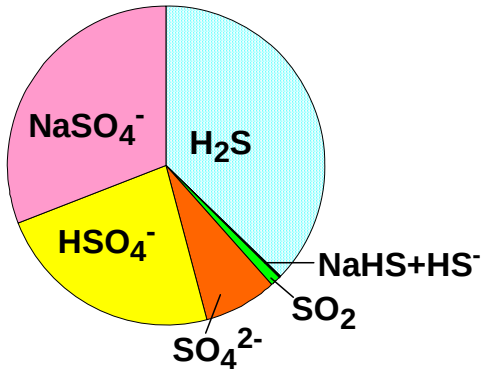

Thermodynamic predictions
(SUPCRT 07)

400°C, 600 bar,
0.5m S - 0.4m NaOH - H_2O, pH ~ 7

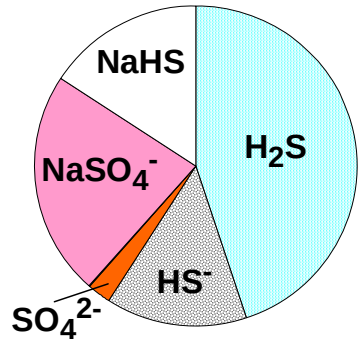

Thermodynamic predictions
(SUPCRT 07)

W6365_revised-Fig. 2

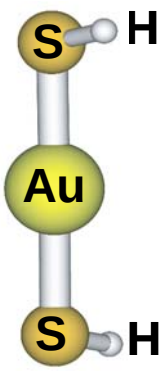

$Au(HS)_2^-$

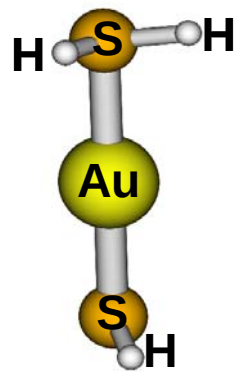

$Au(H_2S)HS^0$, cis

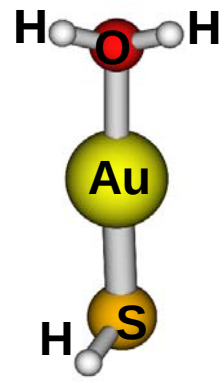

$Au(H_2O)HS^0$, cis
(=$AuHS^0$)

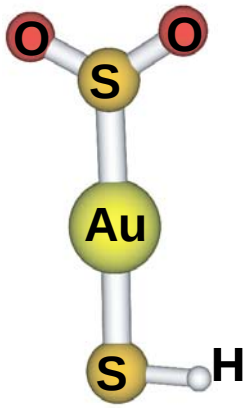

$Au(SO_2)HS^0$

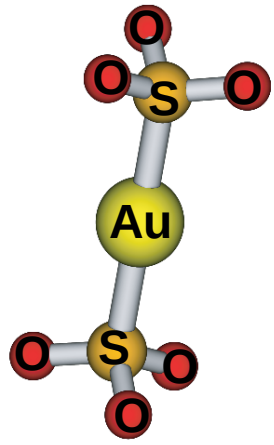

$Au(SO_3)_2^{3-}$

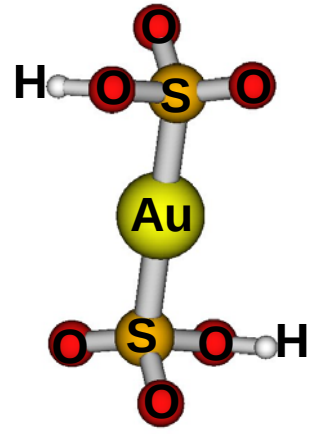

$Au(HSO_3)_2^-$

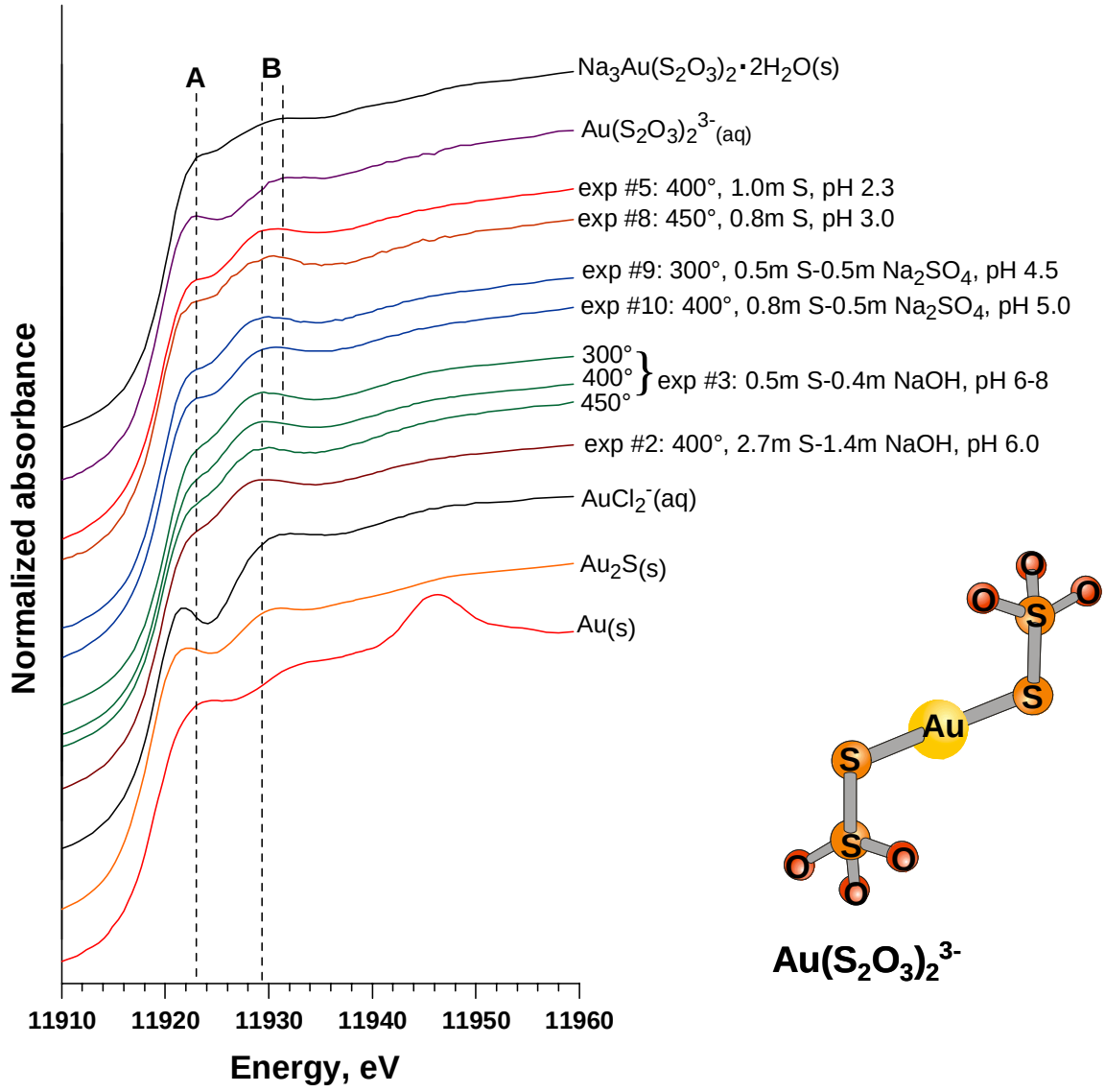

W6365_revised-Fig. 4

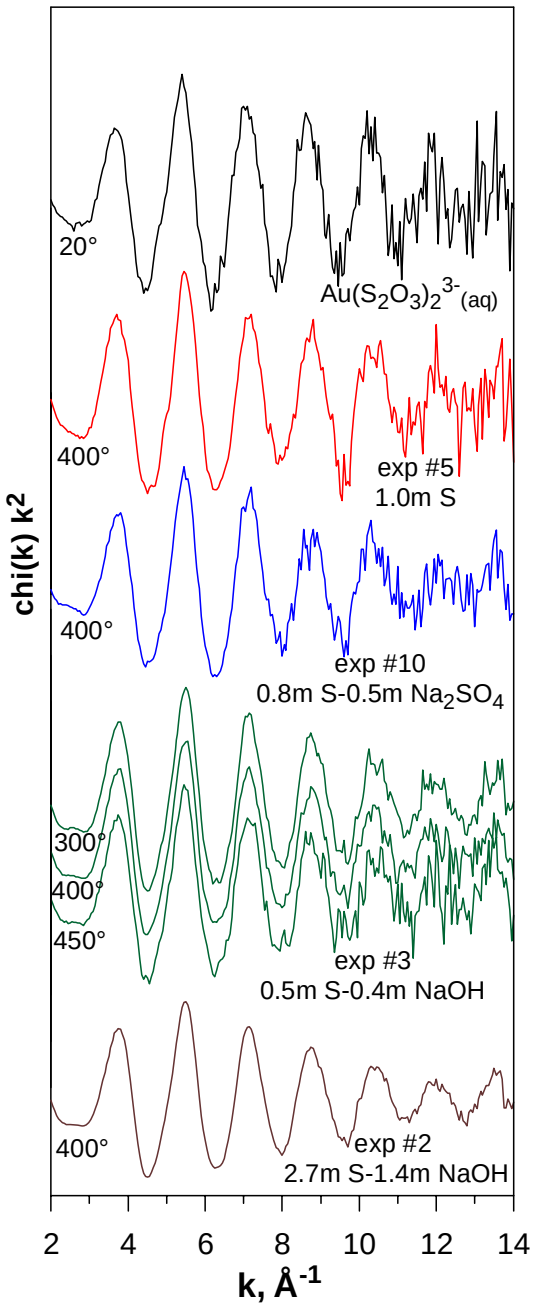

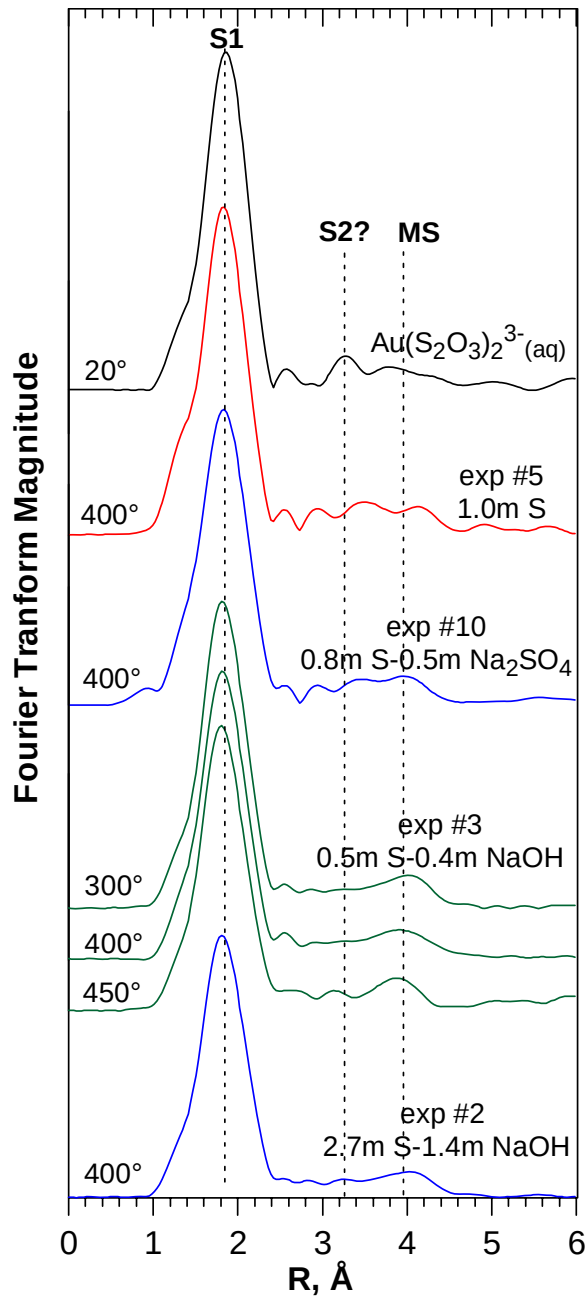

W6365_revised-Fig. 5

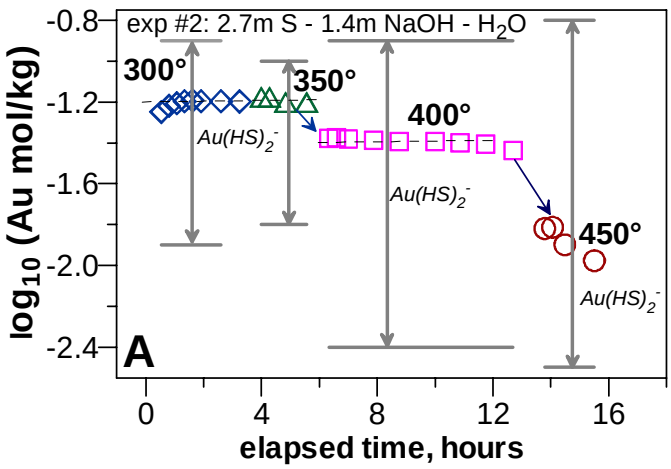

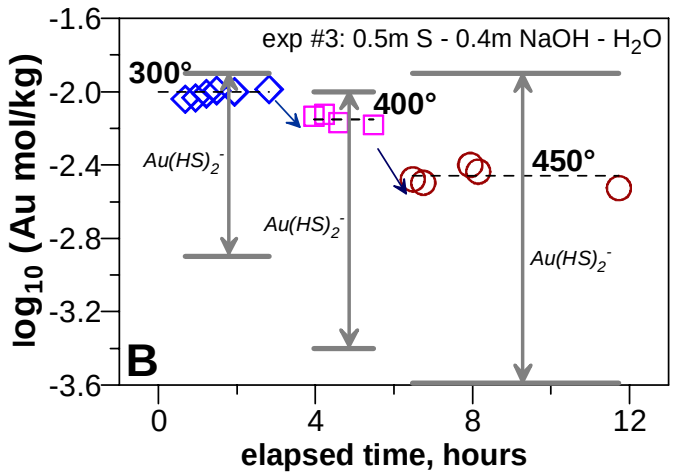

W6365_revised-Fig. 6

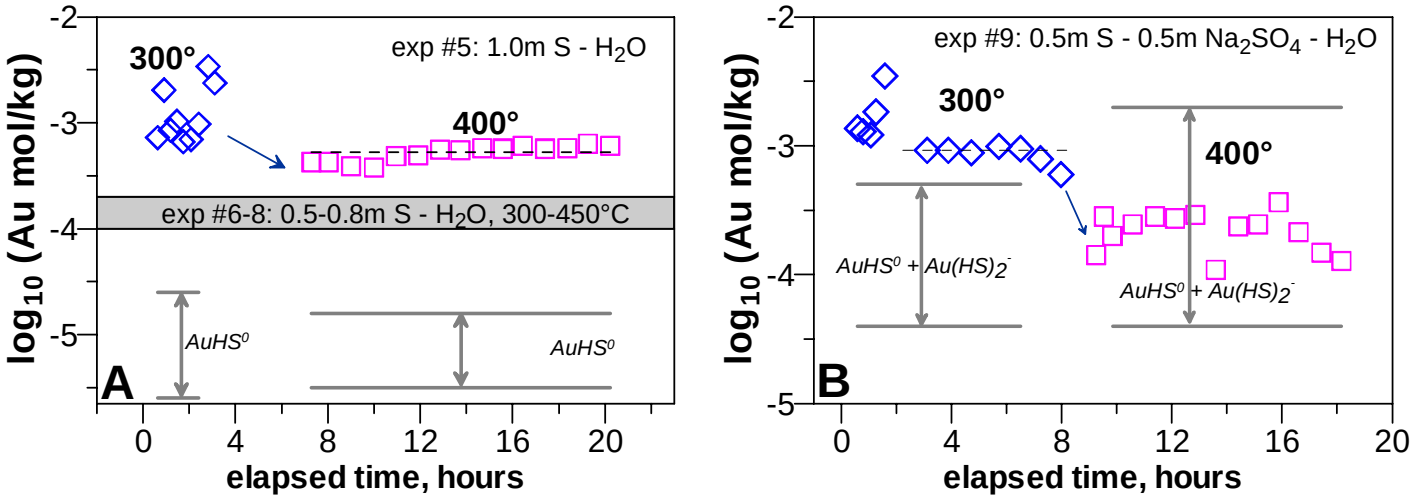

W6365_revised-Fig. 7